THE PLANT CELL

Large-Scale Biology

The dimorphic diaspore model *Aethionema arabicum* (Brassicaceae): Distinct molecular and morphological control of responses to parental and germination temperatures

Jake O. Chandler [ID],[1,†] Per K.I. Wilhelmsson [ID],[2] Noe Fernandez-Pozo [ID],[2,3] Kai Graeber [ID],[1]
Waheed Arshad [ID],[1] Marta Pérez [ID],[1] Tina Steinbrecher [ID],[1] Kristian K. Ullrich [ID],[2,‡]
Thu-Phuong Nguyen [ID],[4] Zsuzsanna Mérai [ID],[5] Klaus Mummenhoff [ID],[6] Günter Theißen [ID],[7]
Miroslav Strnad [ID],[8] Ortrun Mittelsten Scheid [ID],[5] M. Eric Schranz [ID],[4] Ivan Petřík [ID],[8]
Danuše Tarkowská [ID],[8] Ondřej Novák [ID],[8] Stefan A. Rensing [ID],[2,9,*] Gerhard Leubner-Metzger [ID],[1,8,*]

1 Department of Biological Sciences, Royal Holloway University of London, Egham, Surrey TW20 0EX, UK
2 Plant Cell Biology, Faculty of Biology, University of Marburg, Marburg 35043, Germany
3 Institute for Mediterranean and Subtropical Horticulture "La Mayora" (IHSM-CSIC-UMA), Málaga 29010, Spain
4 Biosystematics Group, Wageningen University, PB Wageningen 6708, The Netherlands
5 Gregor Mendel Institute of Molecular Plant Biology, Austrian Academy of Sciences, Vienna Biocenter (VBC), Vienna 1030, Austria
6 Department of Biology, Botany, University of Osnabrück, Osnabrück 49076, Germany
7 Matthias Schleiden Institute/Department of Genetics, Friedrich Schiller University Jena, Jena 07743, Germany
8 Laboratory of Growth Regulators, Faculty of Science, Palacký University and Institute of Experimental Botany, Czech Academy of Sciences, Olomouc 78371, Czech Republic
9 Centre for Biological Signalling Studies (BIOSS), University of Freiburg, Freiburg 79104, Germany

*Author for correspondence: Gerhard.Leubner@rhul.ac.uk (G.L.-M.), stefan.rensing@cup.uni-freiburg.de (S.A.R.)
†Current address: Lancaster Environment Centre, Lancaster University, Lancaster LA1 4YQ, UK
‡Current address: Max Planck Institute for Evolutionary Biology, Department of Evolutionary Biology, 24306 Plön, Germany
The authors responsible for distribution of materials integral to the findings presented in this article in accordance with the policy described in the Instructions for Authors (https://academic.oup.com/plcell/pages/General-Instructions) are: Gerhard Leubner-Metzger (Gerhard.Leubner@rhul.ac.uk) and Stefan A. Rensing (stefan.rensing@cup.uni-freiburg.de).

Abstract

Plants in habitats with unpredictable conditions often have diversified bet-hedging strategies that ensure fitness over a wider range of variable environmental factors. A striking example is the diaspore (seed and fruit) heteromorphism that evolved to maximize species survival in *Aethionema arabicum* (Brassicaceae) in which external and endogenous triggers allow the production of two distinct diaspores on the same plant. Using this dimorphic diaspore model, we identified contrasting molecular, biophysical, and ecophysiological mechanisms in the germination responses to different temperatures of the mucilaginous seeds (M⁺ seed morphs), the dispersed indehiscent fruits (IND fruit morphs), and the bare non-mucilaginous M⁻ seeds obtained by pericarp (fruit coat) removal from IND fruits. Large-scale comparative transcriptome and hormone analyses of M⁺ seeds, IND fruits, and M⁻ seeds provided comprehensive datasets for their distinct thermal responses. Morph-specific differences in co-expressed gene modules in seeds, as well as in seed and pericarp hormone contents, identified a role of the IND pericarp in imposing coat dormancy by generating hypoxia affecting abscisic acid (ABA) sensitivity. This involved expression of

Open Access

morph-specific transcription factors, hypoxia response, and cell wall remodeling genes, as well as altered ABA metabolism, transport, and signaling. Parental temperature affected ABA contents and ABA-related gene expression and altered IND pericarp biomechanical properties. Elucidating the molecular framework underlying the diaspore heteromorphism can provide insight into developmental responses to globally changing temperatures.

Introduction

Fruits and seeds as propagation and dispersal units (diaspores) have evolved an outstanding diversity and specialization of morphological, physiological, and biomechanical features during angiosperm evolution. Coordination of diaspore maturation as well as of diaspore germination timing with environmental conditions is essential for the critical phase of establishing the next generation of plants (Finch-Savage and Leubner-Metzger 2006; Donohue et al. 2010). This is especially critical in annual species that must establish germination and plant growth in a given season or persist as diaspores in the seedbank for germination in a later season (Finch-Savage and Footitt 2017). Seed dormancy, i.e. innate block(s) to the completion of germination of an intact viable diaspore under favorable conditions, is the key regulatory mechanism involved in this timing. Temperature during plant reproduction (parental growth temperature) and temperature sensing by the dispersed diaspore provide input determining dormancy depth, germination timing, and adaptation to climatic change (Walck et al. 2011; Fernandez-Pascual et al. 2019; Batlla et al. 2022; Iwasaki et al. 2022; Zhang et al. 2022).

Most species with dry fruits, including Arabidopsis (Arabidopsis thaliana; Brassicaceae), produce seed diaspores released by dehiscence—spontaneous opening at preformed structures from mature fruits (Mühlhausen et al. 2013). Other species have dry indehiscent (IND) fruits where one or more seeds remain encased by the pericarp (fruit coat). These IND fruits are dispersed by abscission, exemplified by several Brassicaceae species (Lu et al. 2015b; Sperber et al. 2017; Mohammed et al. 2019). The pericarp of these IND fruit diaspores may confer coat-imposed dormancy and delayed germination of the enclosed seeds. While most plants have evolved single types of diaspores that are optimized to the respective habitat, other plants employ a bet-hedging strategy by producing different types of diaspores on the same individual plant.

In these cases of diaspore heteromorphism, seeds and fruits differ in morphology, dormancy and germination properties, ecophysiology, and/or tolerance to biotic and abiotic stresses (Imbert 2002; Baskin et al. 2014; Gianella et al. 2021). This diversity maximizes the persistence of a species in environments with variable and unpredictable conditions. Diaspore heteromorphism evolved independently in 26 angiosperm families and is common in the Asteraceae, Amaranthaceae, and Brassicaceae. Examples of seed dimorphism include the black and brown seed morphs of Chenopodium album and Suaeda salsa (Amaranthaceae), which differ in dormancy

and responses to salinity (Baskin et al. 2014; Liu et al. 2018; Loades et al. 2023). The Cakile clade (Brassicaceae) produces fully IND or segmented, partially IND fruits (Hall et al. 2006). The dimorphic desert annual Diptychocarpus strictus (Brassicaceae) disperses short-lived winged, mucilaginous seeds and long-lived IND siliques each containing about 11 seeds (Lu et al. 2015a). While the ecophysiology of these three dimorphic species is well described, the underpinning molecular mechanisms remain largely unknown.

As a model system to investigate the principles of diaspore dimorphism, we have chosen Aethionema arabicum, a small, diploid, annual, herbaceous species in the sister lineage of the core Brassicaceae, in which seed and fruit dimorphism was associated with a switch to an annual life history (Mohammadin et al. 2017). Genome and transcriptome information is available (Haudry et al. 2013; Nguyen et al. 2019; Wilhelmsson et al. 2019; Arshad et al. 2021; Fernandez-Pozo et al. 2021). Aethionema arabicum is adapted to arid and semiarid environments. Its life history strategy appears to be a blend of bet-hedging and plasticity (Bhattacharya et al. 2019), and it exhibits true seed and fruit dimorphism with no intermediate morphs (Lenser et al. 2016). Two distinct fruit types are produced on the same fruiting inflorescence (infructescence): dehiscent (DEH) fruits with four to six mucilaginous (M^+) seeds and IND fruits each containing a single non-mucilaginous (M^-) seed. Upon maturity, DEH fruits shatter, releasing the M^+ seeds, while the dry IND fruits are dispersed in their entirety by abscission. Dimorphic fruits and seeds differ in their transcriptomes throughout their development and in the mature dry state upon dispersal, and the dimorphic diaspores (M^+ seeds and IND fruits) differ in their water uptake patterns and germination timing (Lenser et al. 2018; Arshad et al. 2019; Merai et al. 2019; Wilhelmsson et al. 2019; Nichols et al. 2020; Arshad et al. 2021). Together, these features qualify Ae. arabicum as a suitable model to investigate the molecular and genetic base of diaspore dimorphism.

Temperature is a main ambient factor affecting reproduction, dormancy, and germination of plants (Walck et al. 2011; Fernandez-Pascual et al. 2019; Batlla et al. 2022; Iwasaki et al. 2022; Zhang et al. 2022), and temperature during reproductive growth is known to affect the ratio of IND/DEH fruit production of Ae. arabicum (Lenser et al. 2016). In our large-scale biology study, we provide a comprehensive comparative analysis of gene expression levels, hormonal status, and biophysical and morphological properties underpinning the distinct Ae. arabicum dimorphic diaspore responses to ambient temperatures. By comparing M^+ seeds dispersed from the fruits by dehiscence, IND fruits containing M^- seeds dispersed by abscission, and bare M^- seeds obtained from IND fruits by manually removing the pericarp, we show that growth
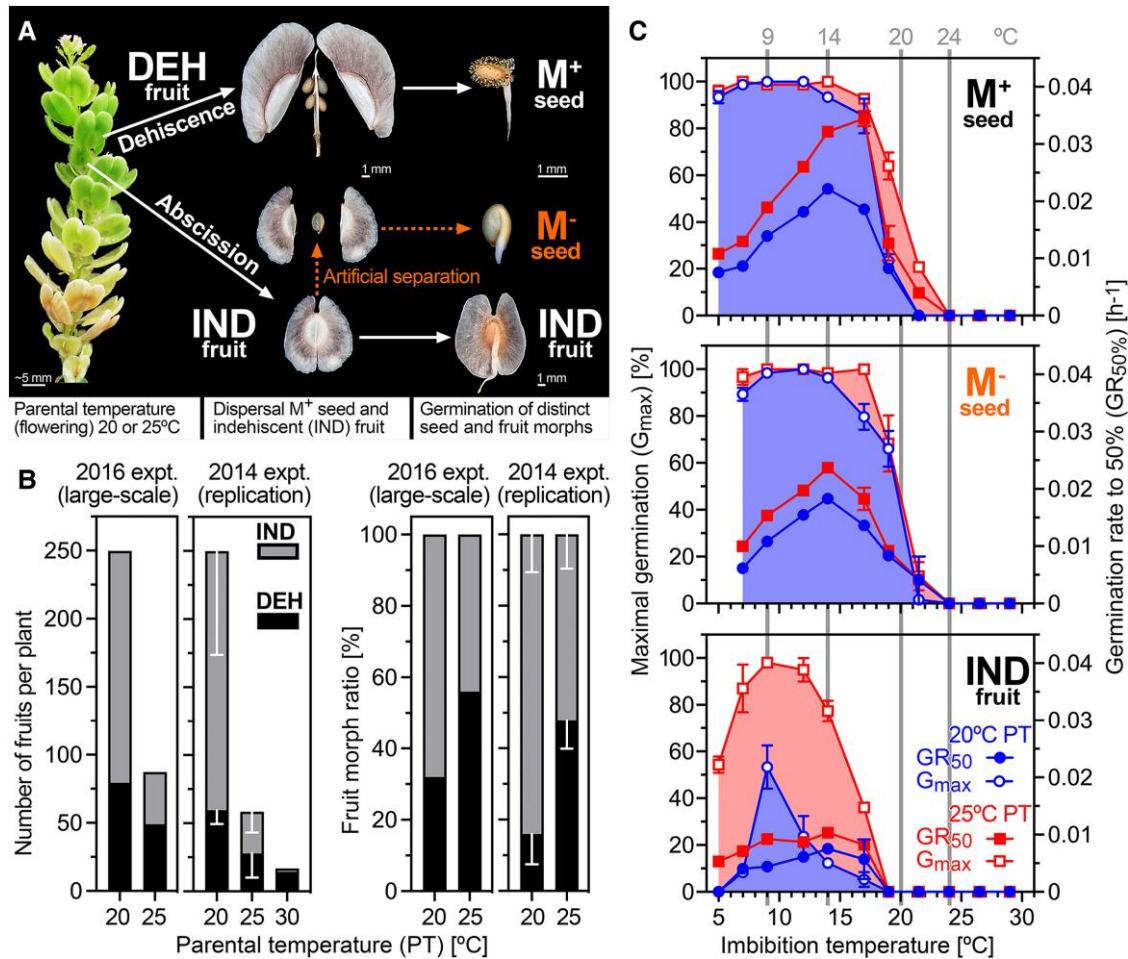
Figure 1. Dimorphic diaspore responses of *Aethionema arabicum* to ambient temperatures. **A)** Infructescence showing two morphologically distinct fruit types. Large, dehiscent (DEH) fruits contain four to six seed diaspores that produce mucilage (M$^+$) upon imbibition. Small, indehiscent (IND) fruits contain a single non-mucilaginous (M$^-$) seed each. For experiments with the bare M$^-$ seed, the pericarp was manually removed. **B)** The effect of parental temperatures (PT; ambient temperatures during reproduction) on the numbers and ratios of the fruit morphs in the 2016 harvest (large-scale) experiment (Supplementary Fig. S1) and the 2014 harvest experiment (mean ± SD values of three replicates; total numbers of fruits were normalized to the large-scale experiment to aid comparison of the relative numbers for IND and DEH; the 20 and 25 °C 2014 harvest was used in the Lenser et al. (2016) publication). **C)** The effect of imbibition temperatures on the maximal germination percentages (G$_{max}$) and the speed of germination expressed as germination rate (GR$_{50\%}$) of the dimorphic diaspores (M$^+$ seeds, IND fruits), and for comparison of bare M$^-$ seeds (extracted from IND fruits by pericarp removal). Sampling temperatures for molecular analyses are indicated. Mean ± SEM values of three replicate plates each with 20 seeds.

temperature during reproduction of the parent plant and a wide range of imbibition temperatures either promote or delay germination. We also demonstrate how the pericarp of the IND fruit morph imposes coat dormancy.

Results

Aethionema arabicum reproductive plasticity and morph-specific responses to parental and imbibition temperatures

As described in the introduction, *Ae. arabicum* disperses two morphologically distinct diaspores (morphs), namely M$^+$ seeds and IND fruits, that are produced on the same inflorescence (Fig. 1A). The larger DEH fruits release several M$^+$ seeds

upon maturation by dehiscence, whereas the smaller IND fruits each containing a single M$^-$ seed are dispersed by abscission (Fig. 1A). Previous work (Lenser et al. 2016) showed that a 5 °C increase in the ambient temperature during reproduction reduced the overall number of fruits and shifted the ratio between the two fruit types toward the DEH type. This parental temperature (PT) effect was confirmed here in a large-scale experiment with ca. 2,000 plants at two PT regimes during reproduction (20 and 25 °C; Fig. 1B and Supplementary Fig. S1A and Table S1). In earlier work (Lenser et al. 2016), we used 14 °C as the imbibition temperature to compare the germination and water uptake kinetics of the dimorphic diaspores from the 20 °C PT regime (20M$^+$ seeds and 20IND fruits). This demonstrated that the germination of seeds enclosed in the 20IND fruits was much delayed

compared to that of $20M^+$ seeds and bare $20M^-$ seeds obtained from the artificial separation of 20IND fruits by pericarp removal (Fig. 1A). In the IND fruit, the pericarp makes up 74.4% of the morph's mass but at maturity does not contain living cells (Arshad et al. 2019, 2020, 2021). The maximal germination percentage (G_{max}) of the 20IND fruits was also much reduced compared to that of $20M^+$ and $20M^-$ seeds imbibed at 14 °C (Lenser et al. 2016), indicating that the pericarp may impose coat dormancy.

Here, we used the material generated in the large-scale experiment (Fig. 1B) with two distinct PTs but otherwise identical growth conditions to address several aspects of the mechanisms underlying the diaspore dimorphism, especially the pericarp-imposed dormancy in a wide range of imbibition temperatures (Fig. 1C). To investigate this pericarp effect closer, we compared the germination-permissive temperature windows of freshly harvested mature M^+ seeds with IND fruits as well as with bare M^- seeds (M^- obtained from IND by pericarp removal), obtained from plants grown at either 20 °C ($20M^+$, 20IND, $20M^-$) or 25 °C ($25M^+$, 25IND, $25M^-$) during reproduction. Seeds and fruits were imbibed at a range of temperatures between 5 and 30 °C, and their G_{max} as well as their germination rates ($GR_{50\%} = 1/T_{50\%}$, a measure for the speed of germination with $T_{50\%}$ being the time required to reach 50% G_{max}) were quantified (Fig. 1C). IND fruits from plants matured at 20 °C had a slower germination speed (lower germination rate, $GR_{50\%}$), a lower G_{max} at germination-permissive temperatures, and a narrower temperature range allowing near optimal germination, compared to M^+ seeds from the same parents. For example, the 20IND fruits reached their highest G_{max} (ca. 50%) at 9 °C but imbibed at even 2.5 °C higher or lower, and only reached 25% germination. On the other hand, the corresponding $20M^+$ seeds reached a G_{max} of above 85% from 5 to 17.5 °C. Pericarp removal demonstrated that $20M^-$ seeds had a similar optimum germination window as the $20M^+$ seeds, confirming the role of the IND pericarp in blocking germination (coat dormancy) at otherwise permissive temperatures for M^+ and M^- seed germination.

M^+ and M^- seeds from plants grown at the 20 or 25 °C PT regimes had similar germination kinetics, although $25M^+$ and $25M^-$ seeds generally had a higher $GR_{50\%}$, and $25M^+$ seeds germinated slightly better at supra-optimal (warmer) temperatures (Fig. 1C). Interestingly, the $25M^+$ seeds germinated much faster ($t_{50\%}$ 29 h) than $20M^+$ seeds when imbibed at 17 °C ($T_{50\%}$ 54 h). Most different were 25IND fruits, which had a much higher G_{max} at germination-permissive temperatures than 20IND fruits (Fig. 1C). 25IND fruits reached 87–98% germination at temperatures between 7 and 12 °C. Nonetheless, removal of the pericarp (IND versus M^-) increased G_{max} and $GR_{50\%}$, especially at supra-optimal temperatures, for example, from 77% to 98% at 14 °C and from 36% to 100% at 17 °C. The pericarp therefore narrowed the permissive germination window by ca. 5 °C at supra-optimal imbibition temperatures irrespective of the PT. Thus, pericarp-imposed dormancy was still evident, although

less extreme in 25IND fruits compared to in 20IND fruits. At germination-permissive imbibition temperatures, the 25IND and 20IND pericarps therefore differed in their coat dormancy-imposing capabilities.

Large-scale RNA-sequencing and hormone quantification to identify morph-specific germination and dormancy mechanisms in *Ae. arabicum*

The contrasting pericarp-imposed dormancy and germination kinetics of M^+, IND, and M^- showed that the two morphs integrate the signal of ambient imbibition temperature differently and suggest that one component is the ambient temperature during the reproduction of the parental plant (Fig. 1). We hypothesized that the different germination responses to imbibition temperatures are mediated, at least in part, by transcriptional and hormonal changes during imbibition. We therefore collected M^+, M^-, and IND samples from plants grown at PTs of 20 and 25 °C, and then subjected the samples to four representative temperatures (9, 14, 20, and 24 °C) during imbibition. In the sampling scheme (Supplementary Fig. S1B), we considered physical (dry seed, 24 h imbibition) and physiological ($T_{1\%}$) times representing the progression of germination. Temperature of 9 °C is the most germination-permissive (G_{max}) for all morphs, still with a strong pericarp effect for 20IND (Fig. 1C and Supplementary Fig. S1C). At 14 °C, M^+ and M^- seed germination is permitted, while particularly 20IND fruit germination is inhibited more than at 9 °C. Therefore, 9 °C was chosen as the temperature under which to further examine the effect of the pericarp. Imbibition at 20 °C represents conditions when germination of all morphs is relatively inhibited, although a parental effect is evident, as $25M^+$ seeds germinate more readily than $20M^+$ seeds. At 24 °C, germination of all diaspores is completely inhibited.

In the RNA-sequencing (RNA-seq) analyses, counts of transcripts for 23,594 genes of *Ae. arabicum* genome version 2.5 (Haudry et al. 2013) were obtained for each sample (Supplementary Data Set 1). To make the transcript abundance data easily and publicly accessible, we generated a gene expression atlas which is implemented in the *Ae. arabicum* genome database (DB; Fernandez-Pozo et al. 2021) at https://plantcode.cup.uni-freiburg.de/aetar_db/index.php. This tool is based on EasyGDB, a system to develop genomics portals and gene expression atlases, which facilitates the maintenance and integration of new data and tools in the future (Fernandez-Pozo and Bombarely 2022). The *Ae. arabicum* gene expression atlas is very interactive and user-friendly, with tools to compare several genes simultaneously and multiple visualization methods to explore gene expression. It includes the transcriptome results of this work (135 datasets), of *Ae. arabicum* RNA-seq work published earlier (Merai et al. 2019; Wilhelmsson et al. 2019; Arshad et al. 2021), and allows adding future transcriptome datasets. It also links to the newest version 3.1 of the *Ae. arabicum* genome annotation and sequence DB (Fernandez-Pozo et al. 2021) and allows linking to
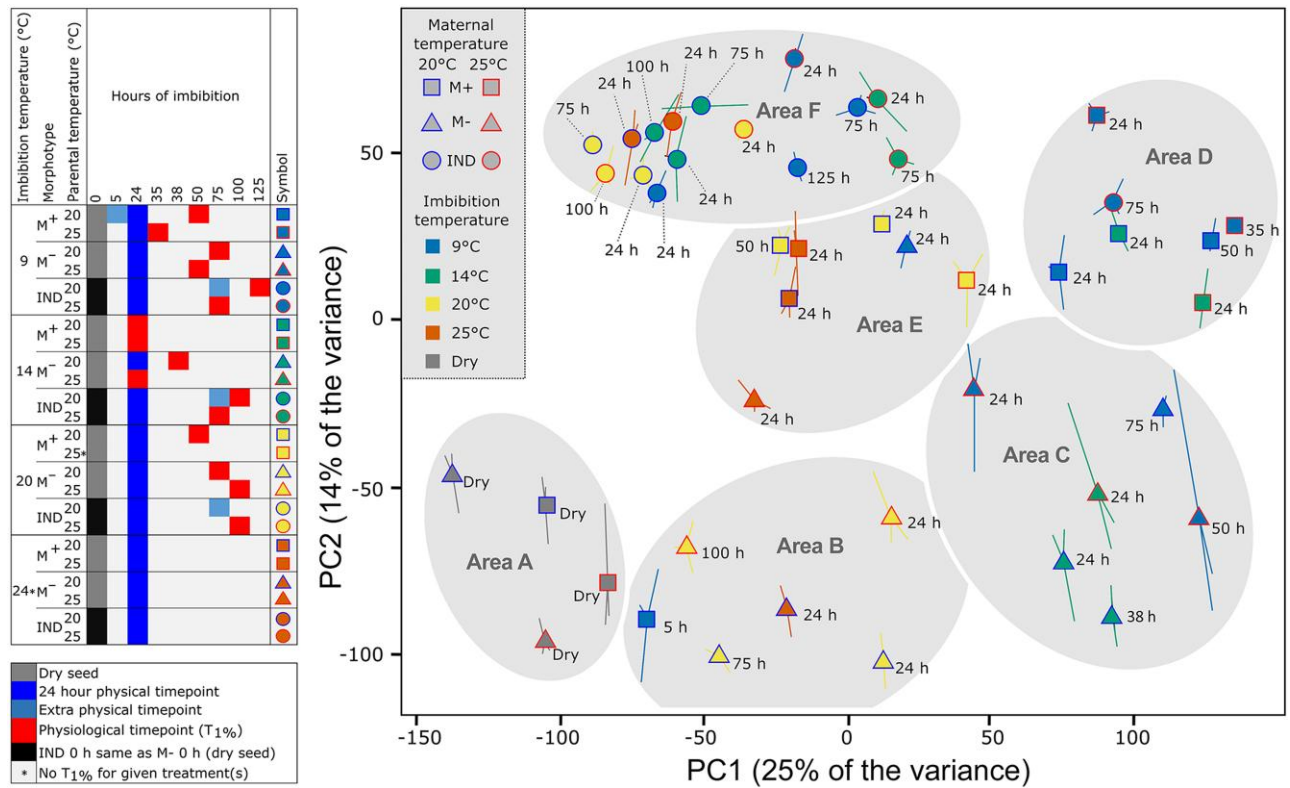
Figure 2. Principal components analysis (PCA) comparing the seed mRNA transcriptome data (RNA-seq analysis) of *Aethionema arabicum*. Mature M^+ and M^- seeds, and IND fruits harvested from plants at two different parental temperatures during reproduction (20 and 25 °C) were sampled in the dry state, and in the imbibed state at four different imbibition temperatures (9, 14, 20, and 24 °C) and times indicated (e.g. 24 h); physiological time points ($T_{1\%}$) are also indicated. Indicated by asterisk, no germination occurred at 24 °C imbibition temperature (precluding $T_{1\%}$ sampling) and $20M^+$ imbibed at 20 °C was sampled only at 24 h. PC1 and PC2 explain 25% and 14% of the variance; for PC3 and individual samples, see Supplementary Fig. S3. Large points indicate average coordinates from three replicates, with the location of each replicate relative to the average shown with a line (some lines are hidden by large points), time point label drop line differentiated by dotted line.

any improved future genome version. Further details and examples for the *Ae. arabicum* gene expression atlas, its analysis, and visualization tools are presented in Supplementary Fig. S2.

Principal component analysis (PCA) based on Log (normalized counts) from 22,200 of 23,594 genes after removing those with zero counts was used to observe general trends in the transcriptomes across the collected samples (Fig. 2 and Supplementary Fig. S3). Prior to imbibition, there were differences in the dry seed transcriptomes, and although these samples cluster together in negative Principal Components PC1 and PC2 coordinates (bottom left, Area A, Fig. 2), a modest number of differentially expressed genes (DEGs) were identified between the samples (Supplementary Data Set 1). For example, there are 322 DEGs between the dry $20M^+$ seed and dry $25M^+$ seed transcriptomes, and 580 DEGs between dry $25M^+$ and dry $25M^-$ seed transcriptomes (Area A, Fig. 2). Therefore, PT and the pericarp (IND versus DEH fruit development) affected the dry seed transcriptomes. A broad trend observed was that following increasing imbibition time, samples from seeds sown under generally germination-permissive conditions traveled positively along PC1 (to Areas C and D, Fig. 2). Samples from seeds sown

under germination-inhibiting conditions stay relatively closer to dry seeds, further supporting that PC1 represents "progress toward completing germination" (Areas B, E, and F, Fig. 2). Reinforcing this, gene expression at an early imbibition timepoint of the $20M^+$ seeds is closer to the "dry seed" state (Area B, Fig. 2). The association between PC1 and final germination percentage is also evident in Supplementary Fig. S3, which provides an extended PCA.

PC2 appears to generally separate IND and M^+ from bare M^- seed, suggesting that PC2 relates to the "pericarp removal" effect on transcriptome changes. However, $20M^-$ imbibed for 24 h at 9 °C are amongst M^+ samples on the PC2 axis (Area E, Fig. 2). In particular, IND fruits under non-germination-permissive conditions form a relatively tight cluster in the negative PC1 and positive PC2 coordinates (Area F, Fig. 2). Interestingly, during the imbibition time course for $20M^-$ and $25M^-$, the 24 h time point is farther along the PC1 axis positively than the later time points (100 h for $25M^-$, 75 h for $20M^-$), indicating the transcriptomes in the later time points resemble that of the dry seed transcriptome more so than the earlier imbibition time points (Area B, Fig. 2). Supporting this, more DEGs were

found between the 24 h $20M^-$ seeds and dry $20M^-$ seeds (4,402) compared to between the 75 h $20M^-$ seeds and dry $20M^-$ seeds (3,822), although there were fewer DEGs between the 24 h $25M^-$ seeds and dry $25M^-$ seeds (3,400) compared to between the 100 h $25M^-$ seeds and dry $25M^-$ seeds (3,913; Supplementary Data Set 1). Indeed, there is more variation than explained by only PC1 and PC2. While PC1 accounts for 25% and PC2 account for 14% of the variance (Fig. 2), PC3 accounts for 11% of the variance and may have some relation to imbibition temperature (Supplementary Fig. S3).

Despite 9 °C imbibition permitting ca. 50% final germination, all imbibed 20IND fruit transcriptomes (24, 75, 125 h) clustered within Area F (Fig. 2). Whereas 25IND fruits imbibed at 9 °C for 24 h were also in Area F, 25IND fruit transcriptomes imbibed at 9 °C for 75 h were in Area D together with the "germinating" transcriptomes of M^+ seed imbibed at 9 and 14 °C. Furthermore, pericarp removal resulted in transcriptomes of M^- seed located in Area C at 75 h, indicating a strong effect of the pericarp on the 20IND fruit transcriptomes (Fig. 2). Thus, it is evident that M^+ and M^- differ in gene expression already in the dry state, and M^+, M^-, and IND differ more so following imbibition. Furthermore, the transcriptomes are strongly influenced by imbibition temperature and pericarp removal. As a whole, the transcriptomes appear to reflect the status in terms of progress toward germination or dormancy, and the presence or absence of the pericarp in the case of seeds from IND fruits.

Co-expressed gene modules in dry and imbibed seed transcriptomes associated with morph-specific germination responses

To further compare gene expression patterns between M^+, M^-, and IND at different imbibition temperatures associated with the regulation of germination progression, we grouped genes by their temperature-, time-, and morph-dependent expression patterns using weighted gene correlation network analysis (WGCNA; Zhang and Horvath 2005). This separated 11,260 expressed genes into 11 modules each containing co-expressed genes (Fig. 3 and Supplementary Fig. S4, gene lists in Supplementary Data Set 2): black (523 genes), blue (1,439), brown (1,373), green (649), gray (2,214), magenta (341), pink (365), purple (259), red (560), turquoise (2,213), and yellow (1,324). Figure 3 shows how neighboring genes in the PCA are clustered together and documents expression of genes in the modules during imbibition at 9 °C. Correlation between expression of genes in the modules and associated PCs, temperatures, traits (morph, $GR_{50\%}$, G_{max}), and quantified seed hormone contents facilitated investigation of potential roles of gene modules in morph-specific germination responses (Fig. 4). Sample traits were clustered by their correlation patterns with module gene expression (using absolute values allowed positive and negative correlations to cluster together). Separation of gene expression patterns into 11 modules allowed identification of enrichment of several key biological processes, including for the largest module (turquoise with 2,213 genes). When put into context of their expression patterns and correlations to trait data, the identified enriched biological processes indicated that modules were of a suitable size to provide meaningful insight into the data, described below.

Expression of purple and turquoise module genes was strongly positively correlated with $GR_{50\%}$ and G_{max}. In contrast, expression of genes in the yellow, green, and red modules was strongly negatively correlated with $GR_{50\%}$ and G_{max}. This suggested that expression of genes in the turquoise and purple modules supports a germination-promoting program. In contrast, expression of genes in the green, yellow, and red modules drives germination prevention or dormancy. Sample PC1 coordinates showed a similar trend reflecting the previously mentioned association between PC1 and germination. Seed abscisic acid (ABA) content, which showed the inverse pattern consistent with its negative association with germination, was highly positively correlated with yellow and green module gene expression and negatively correlated with blue, purple, and turquoise module gene expression. Brown and black module gene expression was highly positively correlated, and the pink module strongly negatively correlated with pericarp presence and PC2. Expression of yellow, green, and red module genes was also positively correlated with imbibition temperature and PC3 (reflecting the association previously mentioned), and purple and turquoise negatively correlated with imbibition temperature. This is consistent with the association between high temperatures and delayed germination. However, the overall correlation trends differed from those with G_{max} and $GR_{50\%}$ demonstrated by tree distance. This can be explained by differences, such as in magenta module gene expression, which were strongly negatively correlated with temperature, but not strongly correlated with germination traits. PT per se was not strongly correlated to any module eigengene.

We further investigated differences in module gene expression between specific sample pairs on a per module basis. Expression of genes in the black module was for example elevated in IND fruits and M^+ seeds compared to in M^- seeds, indicating it is associated with pericarp presence, but not germination kinetics per se, as expression in IND fruits and M^+ seeds is similar despite their contrasting germination kinetics. Expression within the brown module was elevated in IND fruits compared to in both M^+ and M^- at all imbibition temperatures, indicating a morph-specific and pericarp-dependent expression pattern associated with a delay in germination. Expression within the red module was strongly negatively correlated with germination, increased during imbibition under non-permissive germination conditions, and tended to be more highly expressed in IND than M^- (for example, during imbibition at 20 °C). Expression within the green module was strongly correlated with conditions non-permissive for germination: higher in germination-delayed IND than in M^+ and M^- germinating at 9 and 14 °C.
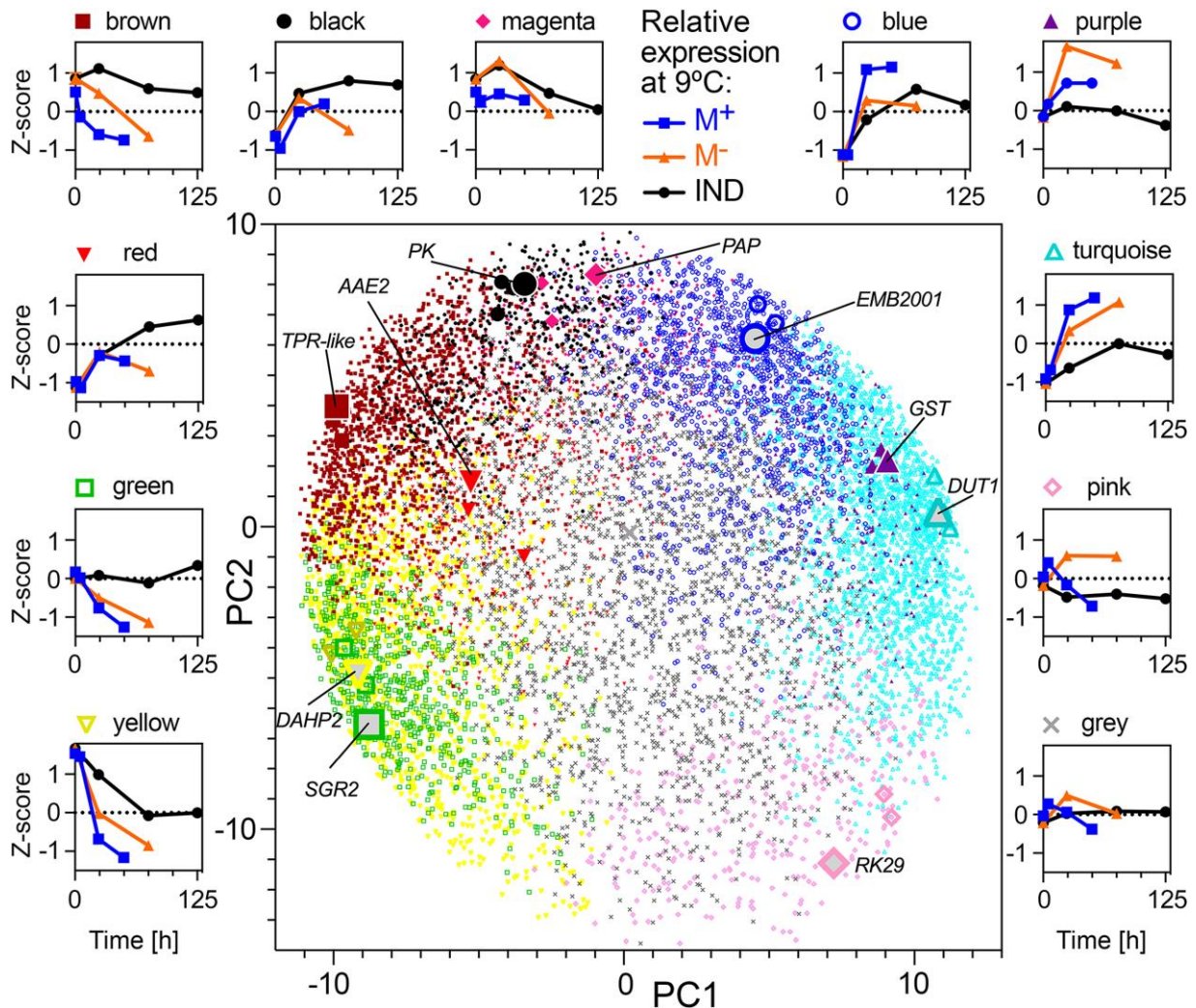
Figure 3. Weighted gene expression correlation network analysis (WGCNA) modules identified from dry and imbibed seed transcriptomes. WGCNA of 11,260 genes identified 11 co-expressed gene modules, identified by color, across mature M⁺ and M⁻ seeds, and IND fruits harvested from plants at two different parental temperatures during reproduction (20 and 25 °C) sampled in the dry state, and in the imbibed state at four different imbibition temperatures (9, 14, 20, and 24 °C) at multiple time points. In the center, genes were separated by PCA of expression across all samples (first two principal components) and colored by module membership. Largest points indicate genes identified with the highest module membership for each module, labeled, and two additional large points representing high module membership candidates for the given module. Outer plots show mean Z-score expression of module genes during imbibition for M⁺ seeds, M⁻ seeds, and IND fruits harvested from plants grown at 20 °C and imbibed at 9 °C. Expression of genes in modules for all samples is shown in Supplementary Fig. S4.

Expression was high in all PT × morphs at 20 °C, perhaps except for 25M⁺, which did indeed germinate better relative to the other PT × morphs at 20 °C. Expression within the green module was higher in 20IND than 25IND at 9 and 14 °C correlating with strength of the pericarp-dependent delay of germination at these temperatures.

Genes within the yellow module were highly expressed in dry seeds compared to in imbibed seeds and also strongly negatively correlated with germination (Figs. 3 and 4). Gene expression decrease in the yellow module over time was delayed under conditions preventing germination and by the presence of the IND pericarp, more in 20IND than 25IND. Yellow module gene expression may be maintained or increased during prolonged inhibition of germination. For

example, yellow module gene expression increased in M⁻ seeds, and perhaps in 20M⁺, imbibed at 20 °C. Inverse to this pattern is the turquoise module where expression was strongly correlated with germination and repressed by the presence of the pericarp, especially in IND fruits from plants grown at 20 °C. Expression within the pink module was strongly correlated with pericarp removal: highly expressed in M⁻ seeds compared to in IND fruit and M⁺ seeds. Compared to other modules, genes in the gray module were more stably expressed across all treatments, but expression correlated positively with germination and negatively with imbibition and imbibition temperature. Genes in the magenta module were expressed more highly at lower than at higher imbibition temperatures, and their expression

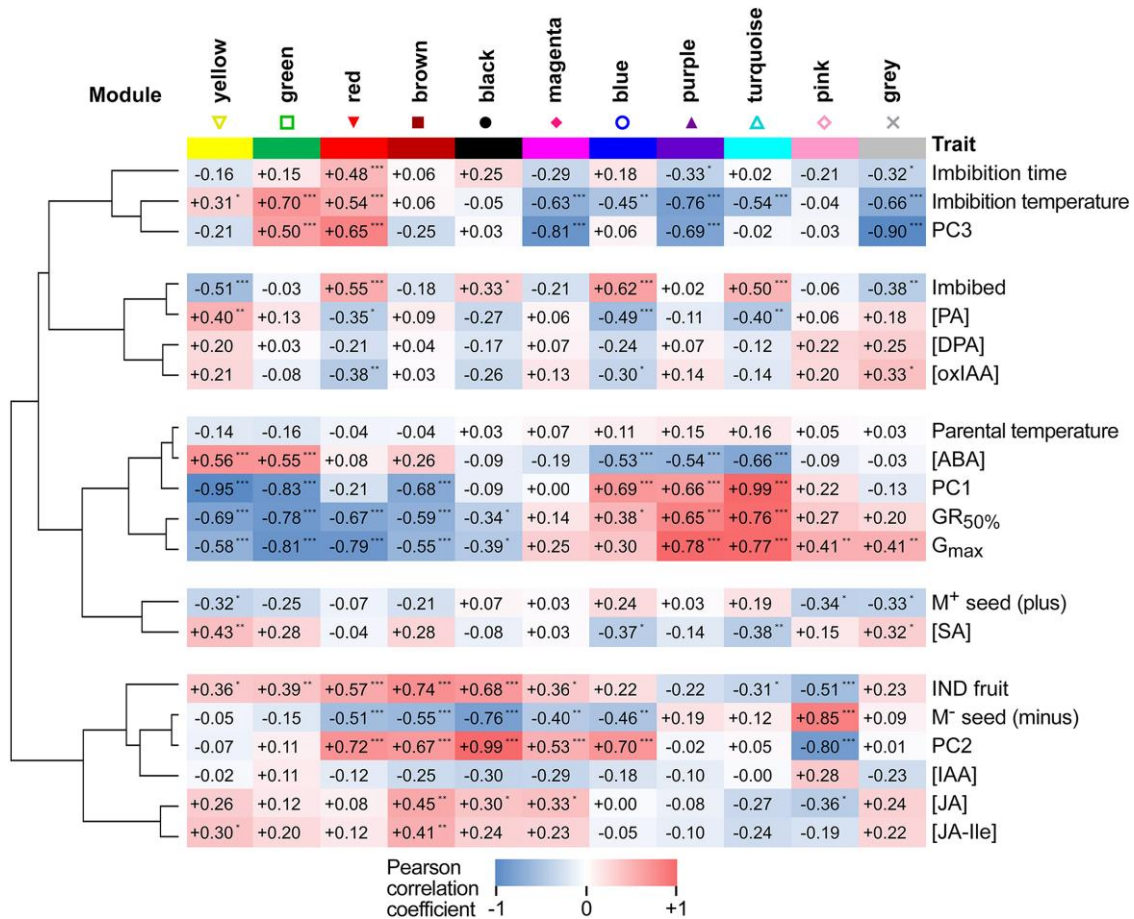| Module	yellow ▽	green □	red ▼	brown ■	black ●	magenta ◆	blue ○	purple ▲	turquoise △	pink ◇	grey ×	Trait
	-0.16	+0.15	+0.48***	+0.06	+0.25	-0.29	+0.18	-0.33*	+0.02	-0.21	-0.32*	Imbibition time
	+0.31*	+0.70***	+0.54***	+0.06	-0.05	-0.63***	-0.45**	-0.76***	-0.54***	-0.04	-0.66***	Imbibition temperature
	-0.21	+0.50***	+0.65***	-0.25	+0.03	-0.81***	+0.06	-0.69***	-0.02	-0.03	-0.90***	PC3
	-0.51***	-0.03	+0.55***	-0.18	+0.33*	-0.21	+0.62***	+0.02	+0.50***	-0.06	-0.38**	Imbibed
	+0.40**	+0.13	-0.35*	+0.09	-0.27	+0.06	-0.49***	-0.11	-0.40**	+0.06	+0.18	[PA]
	+0.20	+0.03	-0.21	+0.04	-0.17	+0.07	-0.24	+0.07	-0.12	+0.22	+0.25	[DPA]
	+0.21	-0.08	-0.38**	+0.03	-0.26	+0.13	-0.30*	+0.14	-0.14	+0.20	+0.33*	[oxIAA]
	-0.14	-0.16	-0.04	-0.04	+0.03	+0.07	+0.11	+0.15	+0.16	+0.05	+0.03	Parental temperature
	+0.56***	+0.55***	+0.08	+0.26	-0.09	-0.19	-0.53***	-0.54***	-0.66***	-0.09	-0.03	[ABA]
	-0.95***	-0.83***	-0.21	-0.68***	-0.09	+0.00	+0.69***	+0.66***	+0.99***	+0.22	-0.13	PC1
	-0.69***	-0.78***	-0.67***	-0.59***	-0.34*	+0.14	+0.38*	+0.65***	+0.76***	+0.27	+0.20	$GR_{50\%}$
	-0.58***	-0.81***	-0.79***	-0.55***	-0.39*	+0.25	+0.30	+0.78***	+0.77***	+0.41**	+0.41**	G_{max}
	-0.32*	-0.25	-0.07	-0.21	+0.07	+0.03	+0.24	+0.03	+0.19	-0.34*	-0.33*	M^+ seed (plus)
	+0.43**	+0.28	-0.04	+0.28	-0.08	+0.03	-0.37*	-0.14	-0.38**	+0.15	+0.32*	[SA]
	+0.36*	+0.39*	+0.57***	+0.74***	+0.68***	+0.36*	+0.22	-0.22	-0.31*	-0.51***	+0.23	IND fruit
	-0.05	-0.15	-0.51***	-0.55***	-0.76***	-0.40**	-0.46**	+0.19	+0.12	+0.85***	+0.09	M^- seed (minus)
	-0.07	+0.11	+0.72***	+0.67***	+0.99***	+0.53***	+0.70***	-0.02	+0.05	-0.80***	+0.01	PC2
	-0.02	+0.11	-0.12	-0.25	-0.30	-0.29	-0.18	-0.10	-0.00	+0.28	-0.23	[IAA]
	+0.26	+0.12	+0.08	+0.45**	+0.30*	+0.33*	+0.00	-0.08	-0.27	-0.36*	+0.24	[JA]
	+0.30*	+0.20	+0.12	+0.41**	+0.24	+0.23	-0.05	-0.10	-0.24	-0.19	+0.22	[JA-Ile]

Pearson correlation coefficient -1   0   +1

Figure 4. Correlation of WGCNA module expression with sample traits (hormone metabolites and PCA coordinates) and clustering. Hormone metabolites included are ABA, ABA degradation products PA and DPA, SA, JA and its isoleucine conjugate (JA-Ile), *cis*-(+)-12-OPDA, IAA and its degradation product 2-ox-IAA (oxIAA). Sample PCA coordinates (PC1, PC2, and PC3) were included as traits. Imbibition time, parental and imbibition temperature, $GR_{50\%}$ and G_{max} of samples were included. M^+ and M^- seeds, and IND fruit (pericarp presence) were included as binary variables (Plus, 0 or 1; Minus, 0 or 1; IND, 0 or 1). Pearson correlation coefficient is indicated by color scale and numbers. Asterisks indicate correlation significance: *$P < 0.05$, **$P < 0.01$, ***$P < 0.001$ according to Student asymptotic P-value for the correlation. Correlation similarity tree was created using hierarchical clustering of absolute correlation coefficient values (1—Pearson, average linkage using Morpheus, https://software.broadinstitute.org/morpheus).

was generally higher in IND than in M^+ or M^- (apart from seeds/fruits from plants grown at 20 °C and imbibed at 9 °C). This module appears to be mostly associated with imbibition temperature.

Expression within the blue module was not generally strongly contrasting dependent on morph or pericarp removal, increased following imbibition, and was generally elevated during imbibition at lower temperatures. Expression within the purple module was strongly positively correlated with germination and negatively with imbibition temperature. Its expression was somewhat opposite of the green module, with high expression associated with germination-permissive temperatures for M^+, M^-, and IND, and higher in 25IND than in 20IND at 9 and 14 °C, also indicating negative association with pericarp-dependent delay of germination.

To gain further insight into which biological processes are associated with the promotion or delay of germination by

morph, pericarp, imbibition temperature, or parental growth temperature, we performed gene ontology (GO) term enrichment analysis of the co-expressed gene modules (Supplementary Data Set 2). This revealed links between expression trends and module gene functions. For example, the GO term "seed dormancy process" was the most enriched in the green module, with "response to ABA" being the 24th most enriched GO term. Other terms enriched in the green and yellow modules were also suggestive of dormancy, for example, "lipid storage" and "chlorophyll catabolic process". Conversely, "translation" was the most enriched GO term in the turquoise module, with a number of cell wall remodeling-related GO terms (e.g. "cell wall pectin metabolic process", "plant-type cell wall organization") and terms suggestive of increased metabolism, promotion of growth and transition to seedling highlighted in the turquoise and purple modules in which expression of the included genes was

positively correlated with germination (e.g. "isopentenyl diphosphate biosynthetic process", "methylerythritol 4-phosphate pathway", "response to cytokinin", "multidimensional cell growth", "photosystem II assembly", "gluconeogenesis", and "glycolytic process"). The selection of specific categories and expression patterns of identified genes presented in the main figures were always complemented with comparisons to their homologs with the same molecular function and/or represented biochemical pathways in the Supplementary Figures.

In summary, out of these 11 gene modules (Fig. 3), four are mainly associated with germination delay (brown, red, green, and yellow); four are associated with germination stimulation (purple, turquoise, pink, and gray); two are associated with imbibition temperature (gray and magenta); one associated mainly with imbibition (blue), four are associated with pericarp presence (black, brown, red, and yellow); and one is associated with pericarp removal (pink). Consistent with module gene functional enrichment and module gene expression correlation with ABA content (Fig. 4), genes related to ABA biosynthesis are, for example, in the yellow, green, and brown modules, for ABA degradation in the blue and gray modules, and ABA receptor genes in the turquoise and purple modules. ABA and cell wall remodeling processes are discussed in more detail below.

The role of the pericarp in altering ABA metabolism and in morph-specific hormonal mechanisms to control dormancy and germination responses to temperature

While obviously many parameters contribute to the control of germination via modified gene expression patterns, the final "decision" depends to a large extent on the level and balance of several plant hormones in A. thaliana (Finch-Savage and Leubner-Metzger 2006; Nambara et al. 2010; Linkies and Leubner-Metzger 2012) and Ae. arabicum (Merai et al. 2019; Merai et al. 2023). We therefore quantified plant hormone metabolites using the same sampling scheme as for the RNA-seq analysis (Supplementary Fig. S1). In the IND fruit, the pericarp makes up 74.4% of the morph's mass but at maturity does not contain living cells (Arshad et al. 2019, 2020, 2021). Transcript abundance patterns for mature dry and imbibed IND fruits therefore represent gene expression changes solely in the M⁻ seed (Lenser et al. 2016; Wilhelmsson et al. 2019; Arshad et al. 2021). The dead IND pericarp however contains hormone metabolites (Lenser et al. 2018) and we therefore quantified the hormone metabolites separately for the two fruit compartments (M⁻ seed and IND pericarp). The pericarp-imposed dormancy of 20IND fruits at 9 and 14 °C imbibition temperature was associated with ABA accumulation in 20M⁻ seeds during the imbibition of intact 20IND fruits (that is ABA content inside M⁻ seeds which were separated from the pericarp *after* imbibition at the times indicated; Fig. 5). In contrast, the ABA contents of 20M⁺ seeds and of bare 20M⁻ seeds (that is ABA content in imbibed M⁻ seeds which were separated from the pericarp *prior* to imbibition, i.e. in the dry state) steadily decreased upon imbibition at permissive temperatures.

In agreement with the high ABA content in seeds, transcript abundance for AearNCED6 (9-cis-epoxycarotenoid dioxygenase), a key gene in ABA biosynthesis, increased in the seeds of imbibed 20IND fruits, and decreased in 20M⁺ and bare 20M⁻ seeds upon imbibition at 9 and 14 °C (Fig. 5). A similar expression pattern was evident for other ABA biosynthesis genes (Supplementary Fig. S5). Consistent with a role of PT, the pericarp-imposed dormancy was reduced in 25IND as compared to in 20IND fruits, and the ABA contents declined in the seeds of imbibed 25IND fruits, as well as in 25M⁺ and bare 25M⁻ seeds upon imbibition at 9 and 14 °C (Fig. 5). Despite this decline, the ABA content in seeds of imbibed 25IND fruits remained higher compared to that of 25M⁺ and 25M⁻ seeds. The observed increase of transcript abundance for AearNCED6 and other ABA biosynthesis genes at 9 and 14 °C imbibition temperature was somewhat reduced in 25IND compared to in 20IND fruits (Fig. 5 and Supplementary Fig. S5). At the non-permissive imbibition temperatures 20 and 24 °C for 20IND and 25IND germination, transcripts for AearNCED6 and other ABA biosynthesis genes accumulated most strongly in seeds of imbibed IND fruits, somewhat in bare M⁻ seeds, but not in M⁺ seeds. At 20 °C imbibition temperature, the ABA content also increased in seeds of imbibed IND fruits and in bare M⁻ seeds, but not in M⁺ seeds. Taken together, these findings suggest that ABA accumulation due to de novo ABA biosynthesis by AearNCED6 and other ABA biosynthesis gene products explains, at least in part, the distinct responses of the morphs to parental and imbibition temperatures, revealing that germination inhibition by elevated ABA levels is a key mechanism of the pericarp-imposed dormancy in 20IND fruits.

In further support of the importance of ABA in the control of the pericarp-imposed dormancy, the enhanced degradation of ABA in the M⁺ seed morph upon imbibition was associated with increased transcript abundances for AearCYP707A3 and other ABA 8′-hydroxylase genes, while their expression remained low in the corresponding IND fruit morph (Fig. 5 and Supplementary Fig. S5). Therefore, the expression patterns of AearCYP707A3 (highest in M⁺ seeds, lowest in IND fruits, intermediate in M⁻ seeds) were, in most cases, inverse to the AearNCED6 expression patterns. Further to this, the expression patterns for gibberellin biosynthesis (GA3-oxidase) and inactivation (GA2-oxidase) genes were inverse to the ABA biosynthesis (NCED) and inactivation (CYP707A) genes (Supplementary Fig. S5D). In addition to ABA metabolism, the presence of the pericarp also enhanced the transcript accumulation for the plasma membrane ABA uptake transporter gene AearABCG40 (an ABC transporter of the G subfamily) and the AearDOG1 (*Delay of germination 1*) dormancy gene in a morph-specific and temperature-dependent manner (Fig. 5).

Hormone metabolite contents per pericarp of ABA, its 8′-hydroxylase pathway breakdown compounds phaseic acid (PA) and dihydrophaseic acid (DPA), as well as for
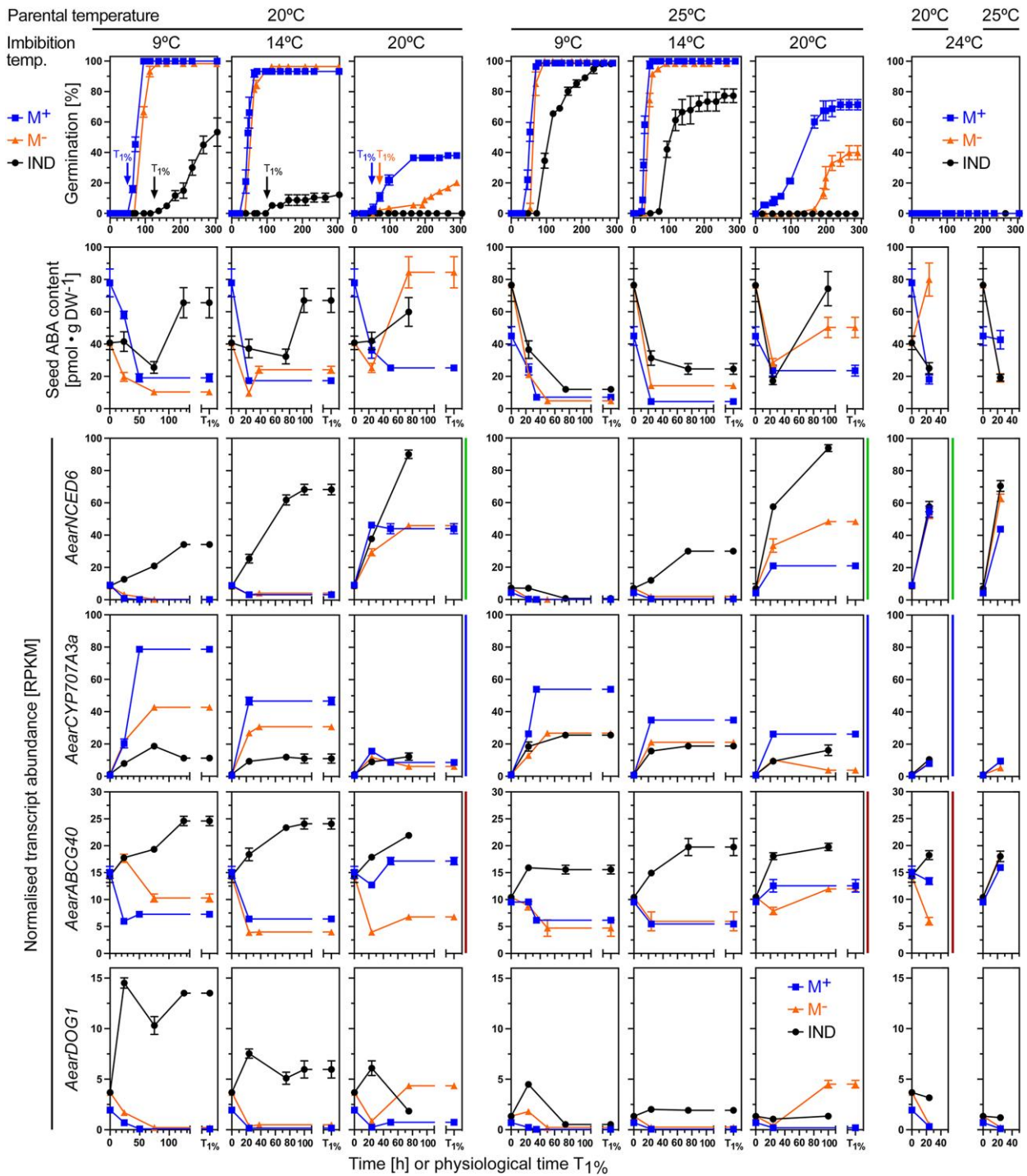
Figure 5. Comparative analysis of germination responses at different temperatures, associated abscisic acid (ABA) content and transcript abundance patterns of *Aethionema arabicum* dimorphic diaspores. Dimorphic diaspores (M⁺ seeds, IND fruits) and bare M⁻ seeds (extracted from IND fruits by pericarp removal) from two parental temperature (PT) regimes during reproduction (20 versus 25 °C) were compared for their germination kinetics, seed ABA contents (M⁺ seeds, bare M⁻ seeds, and M⁻ seeds encased inside the imbibed IND fruit), and seed transcript abundance patterns at four different imbibition temperatures (9, 14, 20, and 24 °C). Comparative results were obtained for physical (in hours) and physiological time points ($T_{1\%}$, representing the population's onset of germination completion). Normalized transcript abundances in RPKM from the transcriptomes (RNA-seq) are presented for the ABA biosynthesis 9-*cis*-epoxycarotenoid dioxygenase gene *AearNCED6*, the ABA 8′-hydroxylase gene *AearCYP707A3*, the plasma membrane ABA uptake transporter gene *AearABCG40*, and the *Delay of germination 1* dormancy gene *AearDOG1*. WGCNA modules (Fig. 3) for these genes are indicated by the vertical color lines next to the graphs. For *Ae. arabicum* gene names and IDs, see Supplementary Table S2 or the Expression Atlas (https://plantcode.cup.uni-freiburg.de/aetar_db/index.php); for RNA-seq single values, see the Expression Atlas or Supplementary Data Set 1. Mean ± SEM values of three (germination, RNA-seq) or five (ABA) replicates each with 20 (germination), 30–40 (ABA), and 60–80 (RNA-seq) seeds are presented.
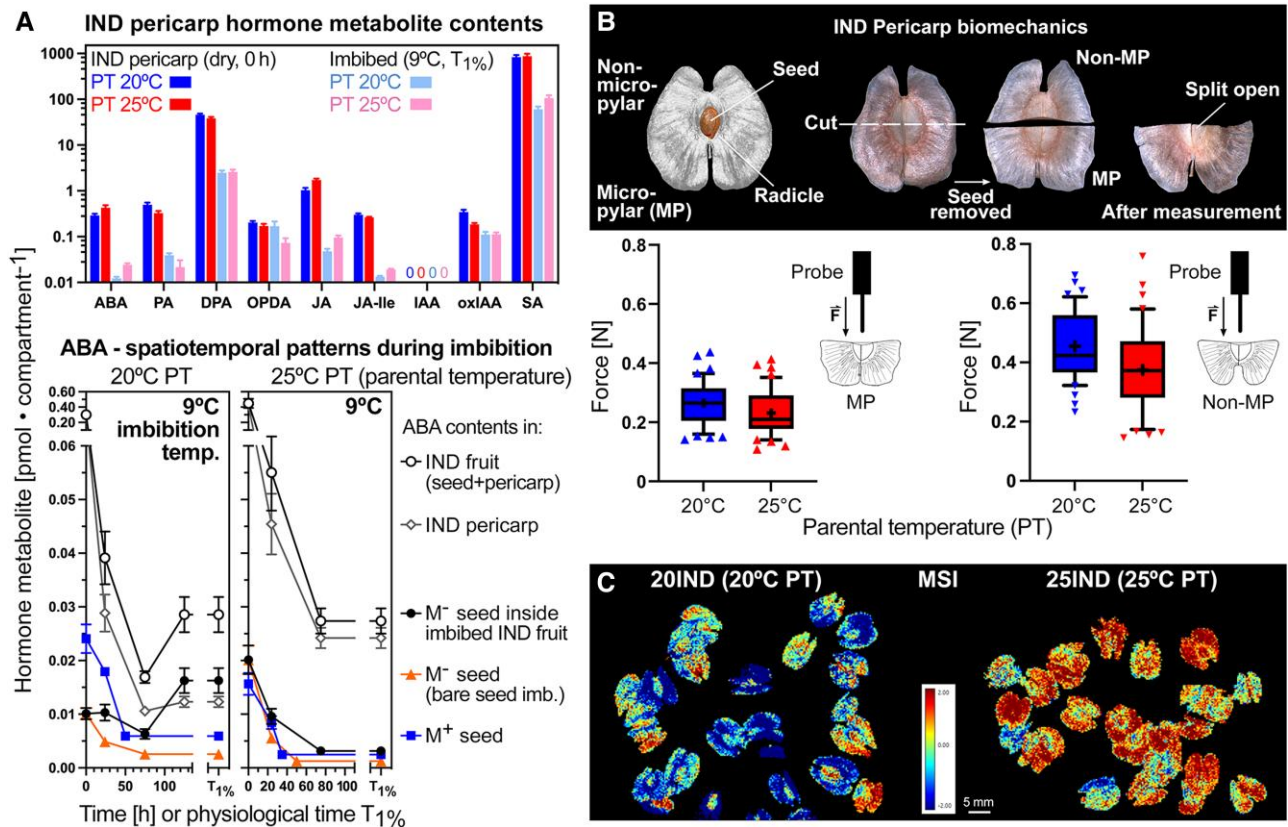
Figure 6. The effect of parental temperature (PT) on the biochemical and biomechanical properties of the IND pericarp and the pericarp-imposed dormancy of *Aethionema arabicum*. **A)** Comparative analysis of hormone metabolite contents in IND pericarps, M⁺ and M⁻ seeds from two PT regimes (20 versus 25 °C) in the dry state and for ABA during imbibition at 9 °C (see Supplementary Fig. S6 for other imbibition temperatures and other hormone metabolites). Hormone metabolites presented: ABA and ABA degradation products PA and DPA, SA, JA and its isoleucine conjugate (JA-Ile), *cis*-(+)-12-OPDA. Mean ± SEM values of five (hormone metabolites) biological replicate samples are presented. **B)** The effect of PT during reproduction on the IND pericarp resistance quantified by biomechanical analysis. Results are presented as box plots, whiskers are drawn down to the 10th percentile and up to the 90th (mean is indicated by "+"), n = 42. The micropylar (where the radicle emerges during fruit germination) pericarp half grown at 20 °C shows a slightly higher tissue resistance versus 25 °C (P = 0.047). The non-micropylar half has a higher tissue resistance while not showing any difference between 20IND and 25IND; see Supplementary Fig. S8 for extended biomechanical properties. **C)** The effect of PT on the IND pericarp biochemical composition as analyzed by multispectral imaging (MSI).

jasmonic acid (JA), its bioactive isoleucine conjugate (JA-Ile) and for salicylic acid (SA), were in general 10–20 fold higher in the dry state and declined rapidly in the pericarp upon imbibition at any temperature (Fig. 6A and Supplementary Fig. S6). In contrast to these hormone metabolites, the content per pericarp of *cis*-(+)-12-oxophytodienoic acid (OPDA), which is an oxylipin signaling molecule and JA biosynthesis precursor (Linkies and Leubner-Metzger 2012; Dave et al. 2016), did not decline during imbibition and its content in the pericarp remained much higher compared to that in the encased M⁻ seed (Supplementary Fig. S6, B and C). When the ABA, PA, DPA, JA, JA-Ile, SA, and OPDA contents of diaspore compartments (seed versus pericarp) were compared, they were, in general, >20 times (dry state) and >5 times (imbibed state) higher in the pericarp compared to in the M⁻ seed extracted from the IND fruit (Fig. 6A and Supplementary Fig. S6). An exception from this was ABA in 20IND fruits where the contents per compartment (pericarp versus encased M⁻ seed) during late imbibition at 9 and

14 °C were roughly equal, but in 25IND fruits ABA was higher in the pericarp compared to in the encased M⁻ seed also during imbibition (Fig. 6A and Supplementary Fig. S6C). Although SA declined rapidly in the pericarp during imbibition, its contents remained much higher in the pericarp also during late imbibition as compared to that in the encased M⁻ seed. Further to this comparison (pericarp versus encased M⁻ seed), the hormone metabolite contents of imbibed bare M⁻ seeds and imbibed M⁺ seeds were always lower compared to that in IND fruits (Fig. 6A and Supplementary Fig. S6). The contents of auxin indole-3-acetic acid (IAA) were low in M⁺ and M⁻ seeds. IAA was below the limit of detection in pericarp tissue, but substantial amounts of the major IAA degradation product 2-oxoindole-3-acetic acid (oxIAA) were detected (Supplementary Fig. S6), suggesting that IAA degradation occurred during the late stages of pericarp development.

Leachates of inhibitors from pericarp tissue, including ABA, OPDA, and phenolic compounds, may inhibit germination and thereby contribute to coat dormancy (Ignatz et al.

2019; Mohammed et al. 2019; Grafi 2020). In agreement with this, pericarp extracts (PEs) and ABA both delayed the germination of bare M⁻ seeds (Supplementary Fig. S7A). PE application explained the delayed 20IND fruit germination only partially, but the delay could be fully mimicked by exposure to 5 μM ABA (Supplementary Fig. S7). Treatment of M⁻ seeds with PE delayed their germination, concordant to the delay of 25IND fruit germination at 9 °C imbibition (Supplementary Fig. S7C). In contrast to PE and ABA, treatment of seeds with SA, OPDA, JA, or JA-Ile did not appreciably affect seed germination (Supplementary Fig. S6D), and PE from 20IND and 25IND pericarps did not differ in their inhibitory effects (Supplementary Fig. S7, C and D). To investigate if PE and ABA treatment of bare M⁻ seeds can mimic the pericarp effect on gene expression as observed in imbibed IND fruits, we conducted reverse transcription-quantitative PCR (RT-qPCR) of representative genes for each WGCNA module. In several cases, the ABA treatment indeed mimicked the PE effect (Supplementary Fig. S7B), but neither PE nor ABA could fully mimic the effect of the intact pericarp. We, therefore, conclude that leaching of ABA or other inhibitors from the pericarp is not the major component by which the pericarp exerts its effects on gene expression and germination responses.

Pericarp properties are known to affect embryo ABA sensitivity, oxygen availability, and the biomechanics of germination (Benech-Arnold et al. 2006; Hoang et al. 2013; Steinbrecher and Leubner-Metzger 2017). Biomechanical analysis revealed that the tissue resistance at the micropylar pericarp (where the radicle emerges during germination of fruit-enclosed seeds) was slightly higher in 20IND as compared to in 25IND pericarps (Fig. 6B and Supplementary Fig. S8). Tissue resistance at the non-micropylar pericarp was higher and did not differ between 20IND and 25IND. PT is also known to affect dormancy via the seed coat pro-anthocyanidin content. Multispectral imaging (MSI) can visualize this and unknown differences in the biochemical composition of seed coats that affect reflectance spectra (Penfield and MacGregor 2017). Figure 6C shows that MSI detected unknown differences in the biochemical composition between 20IND and 25IND fruits. The distinct PTs therefore affected pericarp development leading to distinct biochemical compositions upon maturity. These differences in 20IND and 25IND pericarp biomechanics and biochemistry may also be associated with altered pericarp oxygen permeability. Oxygen plays a key role in the molecular networks regulating seed germination and dormancy, and seed and fruit coat-mediated hypoxia interferes with seed metabolism and hormone signaling in many species (Borisjuk and Rolletschek 2009; Corbineau 2022).

Evidence for pericarp-mediated hypoxia, morph-specific transcription factor expression, and ABA signaling in the control of *Ae. arabicum* dormancy and germination

The complex hypoxia-related regulatory circuitry of hypoxia-responsive genes in angiosperms is characterized by partially conserved transcription factors (TFs), corresponding target *cis*-regulatory elements (TF binding motifs/sites), and specifically stabilization of ethylene response factor (ERF) group VII TF proteins in many species including *A. thaliana* and rice (*Oryza sativa*; Gibbs et al. 2011; Reynoso et al. 2019; Lee and Bailey-Serres 2021). Gasch et al. (2016) identified that promoters of 22 of the identified 49 core hypoxia-responsive genes of *A. thaliana* possess an evolutionary conserved motif, the hypoxia-responsive promoter element (HRPE), spotted by phylogenomic comparison to promoters of putatively orthologous genes of *A. thaliana* relatives. In *A. thaliana*, the ERF group VII has five members: ERF73/HRE1 (HYPOXIA RESPONSIVE ERF1), ERF71/HRE2, RAP2.2 (RELATED TO APETALA2.2), RAP2.3, and RAP2.12. Their roles in inducing their hypoxia-responsive target genes have been well investigated for the fermentation enzymes alcohol dehydrogenase (ADH) and pyruvate dehydrogenase (PDC) (Kürsteiner et al. 2003; Yang et al. 2011; Papdi et al. 2015; Gasch et al. 2016; Seok et al. 2022). Synteny analysis revealed that the angiosperm ERF group VII TFs arose from two ancestral loci with subsequent diversification and duplication (van Veen et al. 2014). Several ERF group VII TFs have also been identified in kiwifruit (*Actinidia* spp.) and their involvement in triggering ADH and PDC gene expression upon waterlogging stress (hypoxia) was demonstrated (Bai et al. 2021; Liu et al. 2022). Recent work by Bai et al. (2024) demonstrated that overexpression of AvERF73 in *A. thaliana* and *Actinidia chinensis* enhances waterlogging tolerance, demonstrating that ERF73 *cis*-elements are similar across the core Eudicots (Rosids and Asterids). Within the Brassicaceae, *A. thaliana* has *AtERF71* and *AtERF73* as two group VII ERF genes, while there is only one homolog in *Ae. arabicum*, a member of the gray module, which we named *AearERF71/73* (*AearHRE1/2*). The translated protein product of AearERF71/73 shares 44% identity with AtERF71 and 31% identity with AtERF73, but less than 25% identity with other closely related ERFs in *A. thaliana* and *Ae. arabicum*. Also, in contrast to *A. thaliana*, which has only one ADH gene (*AtADH1*), there are two ADH genes in *Ae. arabicum*, namely *AearADH1a* (brown module) and *AearADH1b* (green module).

Figure 7A shows that *AearERF71/73* and *AearADH1a* transcripts accumulated in *Ae. arabicum* IND fruits upon imbibition, while their transcript abundances in M⁻ and M⁺ seeds remained low. *AearPDC2* had a similar expression pattern in that the transcript abundances were highest in IND fruits (Supplementary Fig. S9). In contrast to *AearADH1a* and *AearPDC2*, the expression of *AearADH1b* (the second *Ae. arabicum* ADH gene) and *AearPDC1* remained comparatively low, and that of *AearLDH* (*lactate dehydrogenase*) was less consistently elevated in imbibed IND fruits compared to in M⁻ and M⁺ seeds (Fig. 7A and Supplementary Fig. S9). Taken together, this suggested that hypoxia conferred to IND fruits by the pericarp may lead to the induction of the ethanolic fermentation pathway with *AearADH1a* and *AearPDC2* as hypoxia-responsive target genes, which constitutes a hypoxia response as it is known for the *AtADH1* and
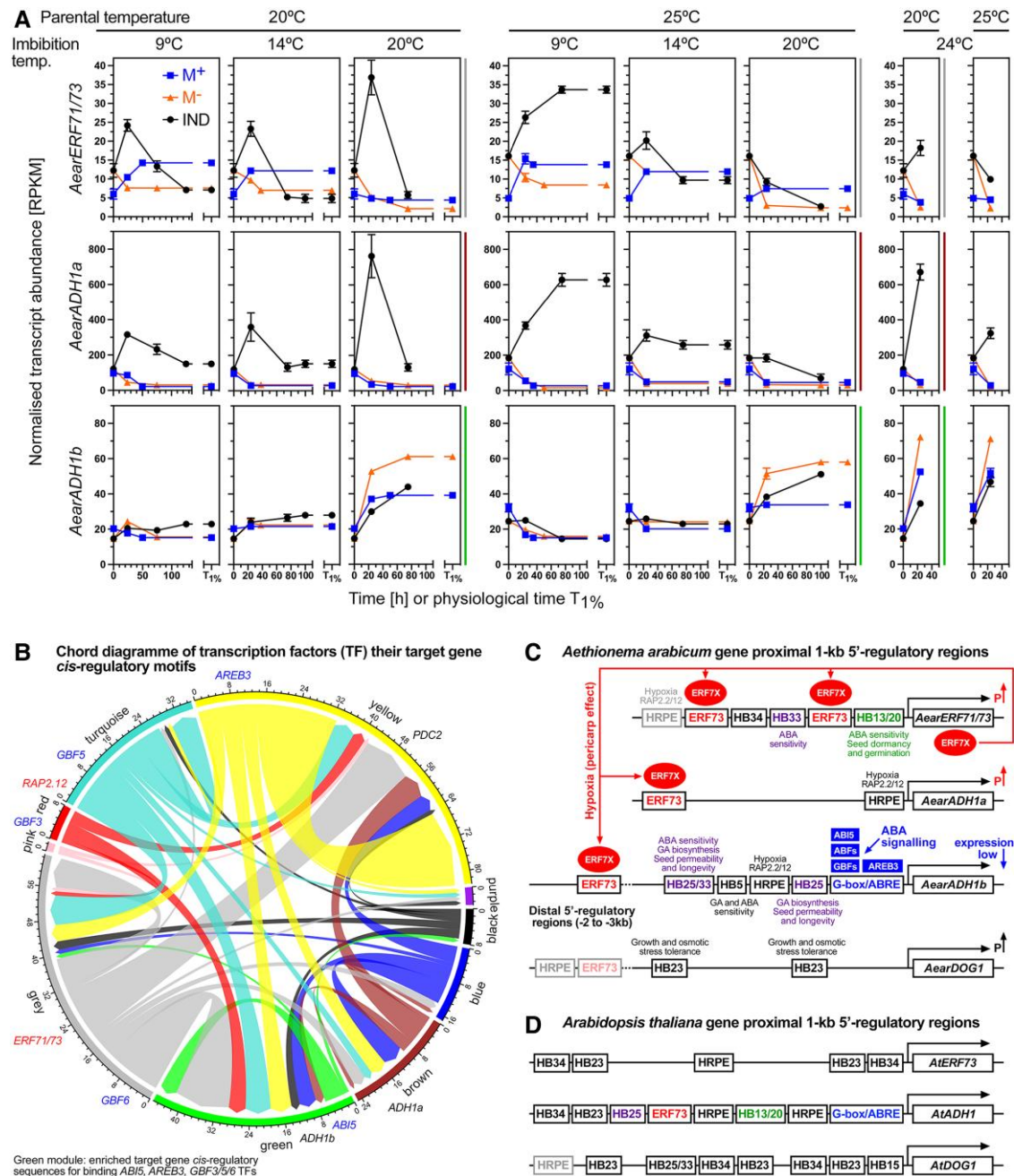
Figure 7. Transcription factor (TF) and target *cis*-regulatory motif analysis of *Aethionema arabicum* gene expression with focus on hypoxia and ABA-related genes. **A)** Transcript abundance patterns (RNA-seq) of the *Ae. arabicum Hypoxia responsive ERF* (*AearERF71/73*) TF gene and the ADH genes *AearADH1a* and *AearADH1b* in seeds of imbibed dimorphic diaspores (M⁺ seeds, IND fruits) and bare M⁻ seeds from two PT regimes (20 versus 25 °C) at four different imbibition temperatures (9, 14, 20, and 24 °C). WGCNA modules (Fig. 3) for these genes are indicated by the vertical color lines next to the graphs. Mean ± SEM values of three replicates each with 60–80 seeds are presented. **B)** Chord diagram of identified TFs and their target genes in the WGCNA modules. Examples for TFs and their target genes. **C)** Hypothetical working model for the pericarp-mediated hypoxia up-regulation (P↑) and ABA signaling, and *cis*-regulatory motifs for the *Ae. arabicum ERF71/73, ADH1a, ADH1b,* and *DOG1* genes. Promoter motifs indicated include the HRPE, the G-box and ABRE, the ERF73 *cis*-regulatory element and HB-motifs for the binding of HB TFs (for details, see Supplementary Fig. S10). These motifs are the targets for the AearERF71/73 TF (ERF7X, *red ellipse*) and the ABA-related ABI5, ABF, GBFs, and AREB3 TFs (*blue boxes*). **D)** Comparative analysis of the corresponding *A. thaliana AtERF73, AtADH1,* and *AtDOG1* gene 5′-regulatory regions (for details, see Supplementary Fig. S10). Note that *A. thaliana* has only one while *Ae. arabicum* has two ADH genes; see Supplementary Fig. S9 for other fermentation-related genes. For *Ae. arabicum* gene names and IDs, see Supplementary Table S2 or the Expression Atlas (https://plantcode.cup.uni-Freiburg.de/aetar_db/index.php); for RNA-seq single values, see the Expression Atlas or Supplementary Data Set 1.

AtPDC1 genes in Arabidopsis seedlings (Kürsteiner et al. 2003; Yang et al. 2011; Papdi et al. 2015; Gasch et al. 2016; Seok et al. 2022). In contrast to the ethanolic fermentation pathway (PDC-ADH, substrate pyruvate), which is up-regulated in IND fruits (Fig. 7 and Supplementary Fig. S9), the seed-specific "Perl's pathway", which controls pyruvate production (Weitbrecht et al. 2011), is down-regulated in IND fruits as compared to in bare M$^-$ seeds (Supplementary Fig. S10). Further examples for hypoxia-regulated genes are presented in Supplementary Fig. S11 and include *AearHRA1*, *AearETR2*, *AearNAC102*, *AearJAZ3*, *AearHHO2*, and other *Ae. arabicum* homologs from the core list of *A. thaliana* hypoxia-responsive genes (Christianson et al. 2009; Gasch et al. 2016; Ju et al. 2019).

To test if *AearERF71/73*, *AearADH1a*, *AearPDC2*, and other candidate genes are indeed regulated by hypoxia, we analyzed their expression in bare M$^-$ seeds imbibed under hypoxia conditions (Fig. 8). Of the 49 core hypoxia-responsive genes in *A. thaliana* seedlings (Gasch et al. 2016), we identified from the transcriptome analysis that expression of 14 of 41 *Ae. arabicum* putative orthologs was elevated in IND fruits, whereas their expression in M$^-$ and M$^+$ seeds remained low (Fig. 7A and Supplementary Figs. S9 and S11). Examples presented in Supplementary Fig. S11 include *AearHRA1*, *AearETR2*, *AearNAC102*, *AearJAZ3*, *AearHHO2*, and other *Ae. arabicum* homologs from the core list of *A. thaliana* hypoxia-responsive genes (Christianson et al. 2009; Gasch et al. 2016; Ju et al. 2019). Figure 8A shows that the germination of bare M$^-$ seeds is indeed severely delayed under hypoxia (4.5% oxygen) as compared to under normoxia (21% oxygen) conditions. This resulted in the hypoxia-mediated induction of *AearERF71/73*, *AearADH1a*, *AearPDC2*, *AearHRA1*, *AearETR2*, *AearJAZ3*, *AearNAC102*, *AearHHO2*, and other genes (Fig. 8A and Supplementary Fig. S12). Hypoxia delayed the germination of bare M$^-$ seeds similar to the pericarp in IND fruits, in both cases the $T_{1\%}$ was ca. 100 h (Supplementary Fig. S12). M$^-$ seed germination was also delayed by 5 μM ABA, and the combined treatment (hypoxia + ABA) had a stronger inhibitory effect on germination (Fig. 8A).

A comparison of several Brassicaceae genomes, including that of *A. thaliana* and *Ae. arabicum*, revealed a high number of conserved noncoding sequences (Haudry et al. 2013). To identify TF genes and corresponding target *cis*-regulatory element candidates in *Ae. arabicum*, we conducted enrichment analyses for each WGCNA module. Enriched motifs from the ArabidopsisDAPv1 DB (O'Malley et al. 2016) for each module are compiled in Supplementary Data Set 3. The chord diagram (Fig. 7B) shows identified *Ae. arabicum* TF genes in each WGCNA module and their connection to corresponding *cis*-regulatory motifs. For example, for ABA-related basic leucine zipper (bZIP) TFs (Nambara et al. 2010) such as ABA Insensitive 5 (ABI5, green module), ABA-responsive element (ABRE)-binding proteins, or ABRE-binding factors (ABFs) such as AREB3 (yellow module), and G-box-binding factors (GBFs) such as GBF3 (red

module), motifs were enriched in the green module (Fig. 7B and Supplementary Data Set 3). The ABRE and HRPE motifs and the TFs binding to these *cis*-regulatory elements are enriched in promoters of hypoxia-responsive and ABA-responsive genes and widely conserved among multiple species (Gomez-Porras et al. 2007; Gasch et al. 2016; O'Malley et al. 2016). Bai et al. (2024) demonstrated that overexpression of *AvERF73* in *A. thaliana* and *A. chinensis* enhances waterlogging tolerance including enrichment in the GO term "cellular response to hypoxia". This work demonstrated that the ERF73 *cis*-elements of these two distantly related species are similar and DNA Affinity Purification and sequencing (DAP-seq) of *A. chinensis* identified a core GCCGCC binding motif which is typical for ERFs (Bai et al. 2024). In *Ae. arabicum*, HRPE and putative ERF73 motifs were enriched in the gray, yellow, and brown modules, and putative target genes *AearADH1a* and *AearPDC2* are gene members of these modules (Fig. 7B and Supplementary Data Set 3).

To investigate the ABA and hypoxia-regulated expression further within the Brassicaceae, we compared the *Ae. arabicum* and *A. thaliana* ADH, PDC, ERF71/73, LDH, and DOG1 genes for putative *cis*-regulatory binding motif homologs using FIMO (Fig. 7, C and D; Supplementary Figs. S9 and S13 and Supplementary Data Set 4). The focus of this analysis was on more general HRPE, ABRE, ERF73, and binding motifs for Homeobox (HB) TFs (see Supplementary Fig. S13A for best possible matches of *cis*-regulatory binding motifs in *Ae. arabicum* genes). The binding motifs for HB TFs were included in this analysis because they are known to control seed-to-seedling phase transition, seed ABA sensitivity, dormancy, longevity and embryo growth in *A. thaliana* (Barrero et al. 2010; Wang et al. 2011; Bueso et al. 2014; Silva et al. 2016; Stamm et al. 2017). The *AearADH1a* and *AearPDC2* 5'-regulatory gene region contain ERF73 and HRPE motifs and are distinct from the *AtADH1*, *AearPDC1*, and *AearADH1b* 5'-regulatory gene regions in that they do not contain G-box/ABRE motifs (Fig. 7C and Supplementary Fig. S9). The *AearERF71/73* 5'-regulatory gene region was also distinct from its *A. thaliana* homologs by the presence of two putative ERF73 motifs, suggesting as a hypothetical working model that the *AearERF71/73* gene possibly provides a positive feedback regulation on the pericarp/hypoxia-mediated *AearADH1a*, *AearPDC2*, and *AearERF71/73* expression (Fig. 7C). Further details of this hypothetical working model, which requires experimental validation in future research, are described and discussed in Supplementary Fig. S9.

The importance of ABA signaling in the control of *Ae. arabicum* pericarp-imposed dormancy of IND fruits was evident in the expression patterns of ABRE-binding (ABI5, AREBs/ABFs) and G-box-binding (GBFs) bZIP TF genes. Transcripts of *AearAREB3a*, *AearAREB3b*, *AearABI5*, *AearABF1*, *AearABF2*, *AearABF3*, *AearABF4*, *AearGBF1*, *AearGBF2*, *AearGBF3*, and *AearGBF4* were up-regulated in M$^-$ seeds inside IND fruits, and in general expressed lowly in isolated M$^-$ seeds and in M$^+$ seeds (Fig. 9 and Supplementary Fig. S14A). By contrast,
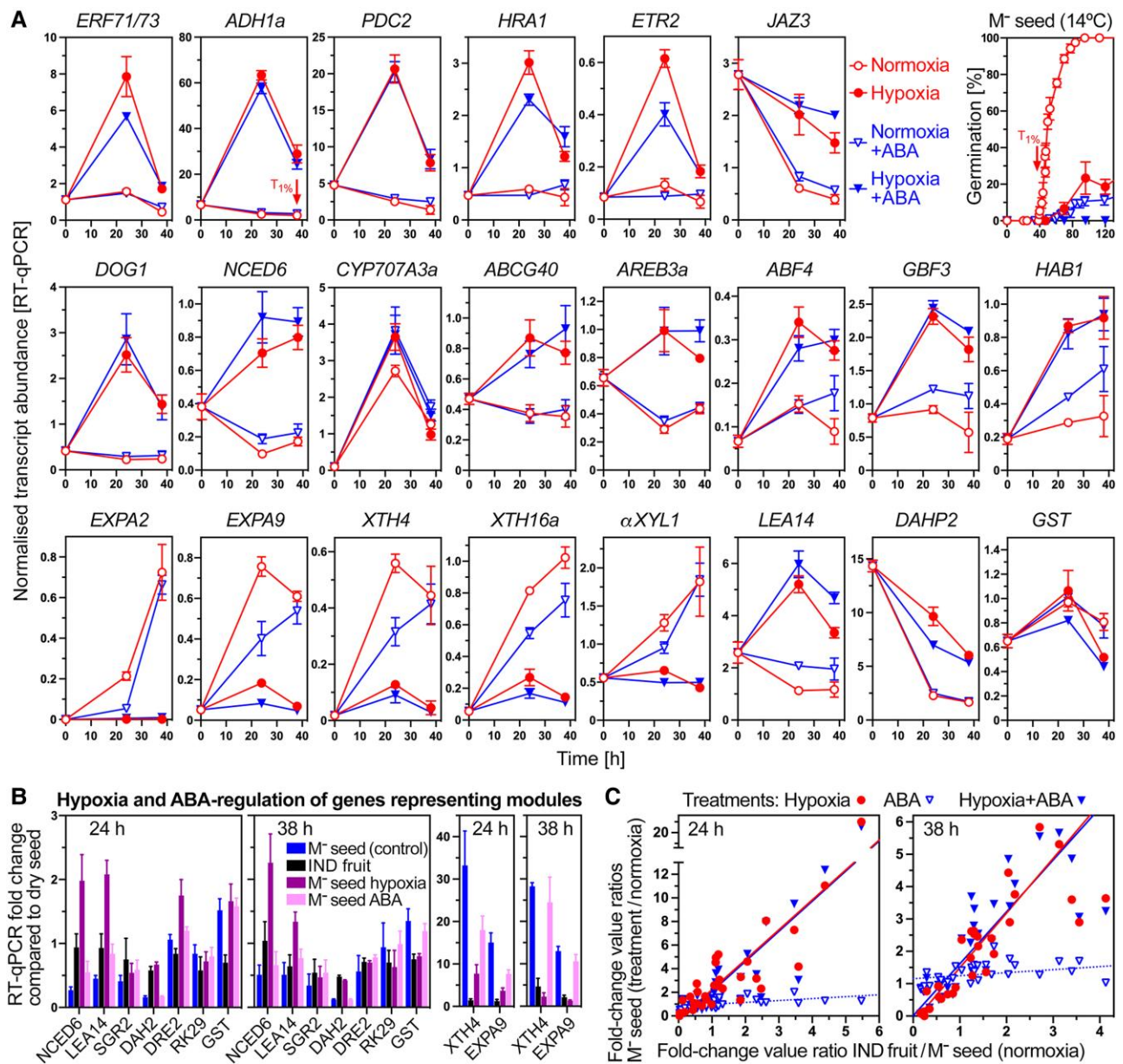
Figure 8. The effect of hypoxia and ABA on germination and gene expression of bare M⁻ seeds. **A)** RT-qPCR expression analysis of selected genes during *Aethionema arabicum* bare M⁻ seed imbibition under hypoxia (4.5 ± 0.2% oxygen) and normoxia (21% oxygen) conditions ± 5 µM ABA. Bare M⁻ seeds were obtained from dry IND fruits by pericarp removal and imbibed at 14 °C in continuous light. The 38 h timepoint (arrow) corresponds to $T_{1\%}$ of the control (normoxia without ABA). For additional genes and expression in IND fruits, see Supplementary Fig. S12. Differential gene expression was assessed using statistical tests (Supplementary Table S4). **B)** RT-qPCR expression analysis of genes representing the WGCNA modules used in Supplementary Fig. S7 to investigate the effects of PE. **C)** Correlation analysis between the effects of the pericarp (IND fruits), hypoxia (M⁻ seeds), and ABA (M⁻ seeds) on the expression of 32 genes as compared to M⁻ seeds in normoxia (control). "Treatments/control" ratios (*y*-axis) of fold-change values (from the dry state to 24 h or 38 h) were calculated and plotted against the "IND fruit/control" ratios (*x*-axis). Linear regression lines indicate strong linear relationships for hypoxia versus pericarp (R^2 0.79 and 0.70 for 38 and 24 h, respectively) and for hypoxia + ABA versus pericarp (R^2 0.80 and 0.75), but not for ABA versus pericarp (R^2 0.16 and 0.30). Mean ± SEM values of three (germination, RT-qPCR) biological replicate samples are presented. For *Ae. arabicum* gene names and IDs, see Supplementary Table S2 or the Expression Atlas (https://plantcode.cup.uni-freiburg.de/aetar_db/index.php).

the transcript abundances of *AearGBF5*, *AearRAP2.12*, and of several HB TF genes including *AearHB13* were down-regulated in M⁻ seeds inside IND fruits (Fig. 9 and Supplementary Fig. S14B). In *A. thaliana*, these bZIP TFs are also known to control

the ABA-related expression, including for the *AtADH1* gene, by binding to G-box and ABRE 5′-regulatory motifs (Lu et al. 1996; Gomez-Porras et al. 2007; Nambara et al. 2010; Yoshida et al. 2010; O'Malley et al. 2016). HB13 and HB20 TFs constitute
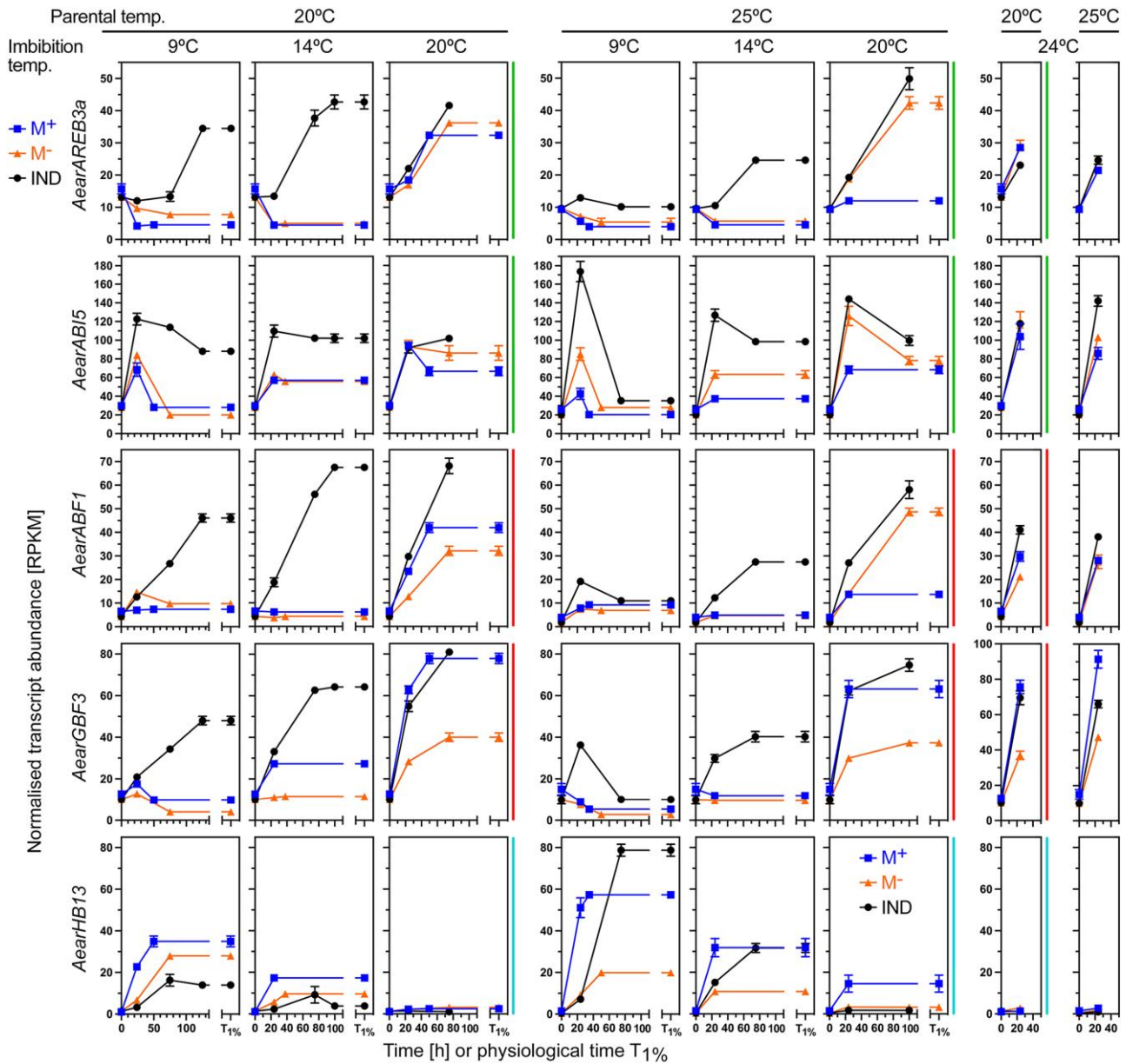
Figure 9. Transcript abundance patterns (RNA-seq) of *Aethionema arabicum* ABA-related and HB TF genes. Results for *AearAREB3a*, *AearABI5*, *AearABF1*, *AearGBF3*, and *AearHB13* transcript abundances in seeds of imbibed dimorphic diaspores (M+ seeds, IND fruits) and bare M− seeds (extracted from IND fruits) from two PT regimes (20 versus 25 °C) at four different imbibition temperatures (9, 14, 20, and 24 °C) are presented (see Supplementary Fig. S14 for other ABF, GBF, and HB TFs). WGCNA modules (Fig. 3) are indicated by the vertical color lines next to the graphs. For *Ae. arabicum* gene names and IDs, see Supplementary Table S2 or the Expression Atlas (https://plantcode.cup.uni-freiburg.de/aetar_db/index.php); for RNA-seq single values, see the Expression Atlas or Supplementary Data Set 1. Mean ± SEM values of three replicates each with 60–80 seeds are presented.

node-regulators within the co-expression network controlling seed-to-seedling phase transition (Silva et al. 2016) while other HB TFs control seed ABA sensitivity, dormancy, longevity, and embryo growth (Barrero et al. 2010; Wang et al. 2011; Bueso et al. 2014; Stamm et al. 2017; Renard et al. 2021). Transcript abundance patterns of ABA signaling component genes including for the protein phosphatase 2C protein HAB1 (Nambara et al. 2010) also exhibit pericarp-affected expression patterns in the *Ae. arabicum* morphs (Supplementary Fig. S14C).

Figure 8A shows that in bare M− seeds imbibed under hypoxia, many ABA-related genes and the dormancy gene *AearDOG1* are up-regulated by hypoxia. In contrast to this, hypoxia or the presence of the pericarp caused down-regulation of genes encoding cell wall remodeling proteins (see next section). Expression of components of the general RNA polymerase II transcription elongation complex, ribosomal proteins, and 20S proteasome subunits differed during *Ae. arabicum* fruit morph development (Wilhelmsson et al. 2019). Related *Ae.*

arabicum genes, especially of the turquoise, purple, and pink WGCNA modules, exhibited distinct pericarp-affected expression patterns (Supplementary Fig. S15), which persisted throughout imbibition.

The role of morph-specific and temperature-dependent expression patterns of cell wall remodeling genes for *Ae. arabicum* germination and dormancy responses

Cell wall remodeling by expansins, and enzymes targeting xyloglucans, pectins, and other cell wall components are required for successful embryo growth and for restraint weakening of covering structures in seed and fruit biology (Graeber et al. 2014; Shigeyama et al. 2016; Steinbrecher and Leubner-Metzger 2017, 2022; Arshad et al. 2021). The expression ratios of expansin genes between M⁻ seed within IND fruit and bare M⁻ seed at 24 h or $T_{1\%}$ remained very low at any imbibition temperature (Fig. 10A and Supplementary Fig. S16A). Consistent with this, transcripts of all *Ae. arabicum* type expansins (Fig. 10C and Supplementary Fig. S16C) were only induced in M⁺ and bare M⁻ seeds, but not appreciably in imbibed IND fruits. Similar results were obtained for xyloglucan *endo*-transglycosylases/hydrolases (XTHs) for 20IND fruits, whereas considerable induction was observed for 25IND fruits at the permissive imbibition temperatures (9 and 14 °C). In addition to XTHs, xyloglucan remodeling is achieved by a battery of bond-specific transferases and hydrolases (Fig. 10B), and in the *Ae. arabicum* transcriptomes, most of them belong to the turquoise WGCNA module with *αXYL1* as an example (Fig. 10). Higher transcript expression in bare 20M⁻ seeds as compared to in 20IND fruits was observed for *αFUCs*, *βGALs*, *βXYL*, and *GATs* (Supplementary Fig. S16D), suggesting that the pericarp-mediated repression and the resultant reduction in xyloglucan remodeling are part of the 20IND dormancy mechanism. The induction in 25IND fruits that eventually germinate further supports the importance of these genes and their products in the germination process. Expression comparison of M⁺ seeds and isolated M⁻ seeds further confirm that the presence of the pericarp is the most important factor for the expression differences between the dimorphic diaspores.

In contrast to the observed hypoxia-induced expression of many genes, hypoxia inhibited the expression of expansin, XTH, and *αXYL1* cell wall remodeling genes in imbibed bare M⁻ seeds (Fig. 8A). Compared to hypoxia, ABA was far less effective and did not appreciably inhibit the induction of the accumulation of *AearEXPA2*, *AearEXPA9*, *AearXTH4*, *AearXTH16a*, and *AearαXYL1* transcripts. The pericarp effect on the gene expression patterns (IND fruits versus bare M⁻ seeds) observed in the transcriptome analysis was confirmed in a completely independent RT-qPCR experiment for these cell wall remodeling genes and for most of the 32 genes investigated (Supplementary Fig. S12C). While for the representative genes for each WGCNA module PE did not affect the gene expression of

bare M⁻ seeds (Supplementary Fig. S12C), hypoxia conditions affected it for about half of the representative genes (Fig. 8B). Correlation analysis between the pericarp effect imposed on M⁻ seeds in imbibed IND fruits and the hypoxia and ABA effects on imbibed bare M⁻ seeds was conducted for the 32 genes of the RT-qPCR experiment (Fig. 8C). This revealed strong linear relationships (R^2 0.7–0.8) for hypoxia versus pericarp, and hypoxia + ABA versus pericarp, but not for ABA alone versus pericarp. Taken together, hypoxia generated by the pericarp seems to be the most important mechanism of the pericarp-mediated dormancy of IND fruits, it seems to act upstream of ABA and affects the gene expression in M⁻ seed encased by the pericarp to control the observed distinct dormancy and germination responses at the different imbibition temperatures.

Discussion

Aethionema arabicum seed and fruit dimorphism: large-scale molecular data sets reveal diaspore bet-hedging strategy mechanisms in variable environments

Ambient temperature during seed reproduction (PT) and after dispersal (including imbibition temperature) is a major determinant for fecundity, yield, seed germinability (i.e. nondormancy versus dormancy of different depths), and environmental adaptation. The effect of temperature variability has been well studied in monomorphic annual plants and mechanisms underpinning the germinability of the dispersed seeds were elucidated (Donohue et al. 2010; Finch-Savage and Footitt 2017; Fernandez-Pascual et al. 2019; Iwasaki et al. 2022; Zhang et al. 2022). In contrast to monomorphic species, very little is known about the morphological and molecular mechanisms that facilitate survival of heteromorphic annual species. Diaspore heteromorphism is a prime example of bet-hedging in angiosperms and is phenologically the production by an individual plant of two (dimorphism) or more seed/fruit morphs that differ in morphology, germinability, and stress ecophysiology to "hedge its bets" in variable (unpredictable) environments (Imbert 2002; Baskin et al. 2014; Gianella et al. 2021).

An advantage of *Ae. arabicum* as a model system is that it exhibits true seed and fruit dimorphism with no intermediate morphs (Lenser et al. 2016). Our earlier work revealed molecular and morphological mechanisms underlying the dimorphic fruit and seed development (Lenser et al. 2018; Wilhelmsson et al. 2019; Arshad et al. 2021), the distinct dispersal properties of the M⁺ seed and IND fruit morphs (Arshad et al. 2019, 2020; Nichols et al. 2020), and the adaptation to specific environmental conditions (Mohammadin et al. 2017; Bhattacharya et al. 2019; Merai et al. 2019; Merai et al. 2023). Transcriptome and imaging analyses of the seed coat developmental program of the mucilaginous *Ae. arabicum* M⁺ seed morph revealed that it resembles the "default" program known from the mucilaginous seeds of *A. thaliana*, *Lepidium sativum*, and other Brassicaceae
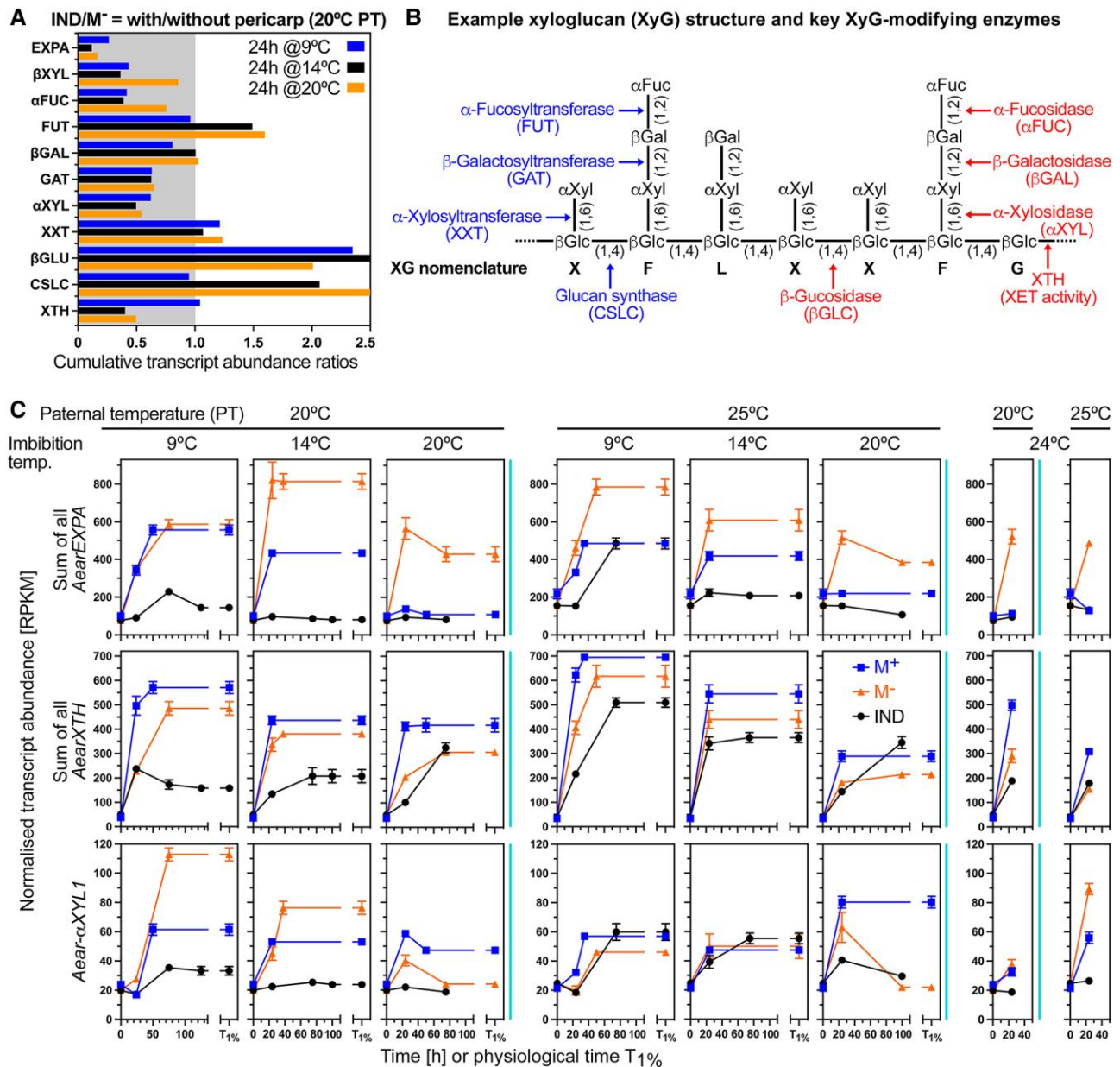
Figure 10. Transcript abundance patterns (RNA-seq) of *Aethionema arabicum* cell wall remodeling protein genes in seeds of imbibed dimorphic diaspores (M⁺ seeds, IND fruits) and bare M⁻ seeds. **A)** Effect of the pericarp on the expression ratios of expansin A and xyloglucan-related cell wall remodeling protein genes in the M⁻ seeds of 24 h imbibed IND fruits and isolated M⁻ seeds. **B)** Xyloglucan remodeling is achieved by a battery of enzymes specifically targeting different bonds of xyloglucan structure as indicated. Among them are XTHs with xyloglucan endotransglucosylase (XET) enzyme activity (Holloway et al. 2021). **C)** Transcript abundance patterns of *Ae. arabicum* expansins A), XTHs, and the α-xylosidase *Aear-αXYL1* in M⁺ seeds, IND fruits and isolated M⁻ seeds from two PT regimes (20 versus 25 °C) at four different imbibition temperatures (9, 14, 20, and 24 °C). For other expansin and xyloglucan-related genes and *Ae. arabicum* gene IDs, see Supplementary Fig. S16 or the Expression Atlas (https://plantcode.cup.uni-freiburg.de/aetar_db/index.php); for RNA-seq single values, see the Expression Atlas or Supplementary Data Set 1. WGCNA modules (Fig. 3) are indicated by the vertical color lines next to the graphs. Mean ± SEM values of three replicates each with 60–80 seeds are presented.

(Graeber et al. 2014; Scheler et al. 2015; Lenser et al. 2016; Arshad et al. 2021; Steinbrecher and Leubner-Metzger 2022). In contrast to this, the non-mucilaginous *Ae. arabicum* M⁻ seed morph resembles *A. thaliana* seed mucilage mutants and thereby highlights that the dimorphic diaspores

enable the comparative analysis of distinct developmental programs without the need for mutants. *Arabidopsis thaliana* accessions differ in depth of their primary seed dormancy, ranging from deep physiological dormancy to shallow dormancy (Cadman et al. 2006; Barrero et al. 2010; Finch-Savage

and Footitt 2017); and *L. sativum* seeds are completely non-dormant (Graeber et al. 2014). During seed imbibition, distinct transcriptional and hormonal regulation either leads to the completion of germination or to dormancy maintenance for which ABA metabolism and signaling, *DOG1* expression, downstream cell wall remodeling, and seed coat properties are key components (Finch-Savage and Leubner-Metzger 2006; Graeber et al. 2014; Footitt et al. 2020; Iwasaki et al. 2022). The transcriptome and hormone data for *Ae. arabicum* M$^+$ seeds confirmed these mechanisms and their dependence on the imbibition temperature to either mount a germination or a dormancy program typical for mucilaginous seeds (Cadman et al. 2006; Scheler et al. 2015; Iwasaki et al. 2022). The *Ae. arabicum* dimorphic diaspore comparison of these M$^+$ seeds to IND fruits (and the bare M$^-$ seeds) revealed how the pericarp of the IND fruit morph imposes the observed coat dormancy.

Pericarp-imposed dormancy: comparative analyses of IND fruit and seed morph germinability reveals mechanisms and roles in thermal responses

The typical Brassicaceae fruit is DEH, opens during fruit maturation (dehiscence, *A. thaliana* seed, *Ae. arabicum* M$^+$ seed morph), and is considered to represent the ancestral fruit type (Mühlhausen et al. 2013). Nevertheless, mono-morphic species that disperse various IND fruit types by abscission evolved many times independently within the Brassicaceae. Different roles of the pericarp in these dry IND Brassicaceae diaspores (siliques and silicles) were identified, including dispersal by wind, persistence in the seed bank, retaining seed viability, delaying water uptake, releasing alle-lochemicals, and imposing coat dormancy (Mamut et al. 2014; Lu et al. 2015b, 2017a, 2017b; Sperber et al. 2017; Mohammed et al. 2019; Khadka et al. 2020). Many of these monomorphic Brassicaceae species with IND fruits are desert annuals. Their IND diaspores have not been investigated for the molecular mechanisms responding to distinct parental and imbibitional temperatures. The *Ae. arabicum* dimorphic diaspore system with its single-seeded IND fruit morph pro-vides an excellent system for investigating these mechanisms.

The pericarp of mature *Ae. arabicum* IND fruits is dead tis-sue that contains high amounts of ABA, OPDA, JA, JA-Ile, and SA, as well as degradation products of ABA and IAA. Leaching of these and other compounds into the fruit's proximal en-vironment could have roles in allelopathic interactions, as de-scribed for the dead pericarp of other species (Grafi 2020; Khadka et al. 2020). Leaching of pericarp inhibitors into the encased seed could also delay fruit germination or confer "chemical coat dormancy", as demonstrated for pericarp-derived ABA in *Lepidium draba* (Mohammed et al. 2019), *Beta vulgaris* (Ignatz et al. 2019), and *Salsola komarovii* (Takeno and Yamaguchi 1991). PEs of *Ae. arabicum* IND fruits as well as ABA delayed M$^-$ seed germination, but they could not fully mimic the pericarp-imposed dormancy and effect on gene expression (Fig. 5). Acting as a mechanical

restraint to water uptake and/or radicle protrusion is an-other way by which the pericarp may delay germination or confer "mechanical coat dormancy" (Sperber et al. 2017; Steinbrecher and Leubner-Metzger 2017). The *Ae. arabicum* IND pericarp is water-permeable (Lenser et al. 2016), and we showed here that it weakens during imbibition. *Aethionema arabicum* pericarp-imposed dormancy was enhanced by the lower PT (20 °C, 20IND fruits) as compared to the higher PT (25 °C, 25IND fruits). This altered the pericarp biochemically and its mechanical resistance, which was higher in 20IND pericarps (Fig. 6), as was the pericarp-imposed dormancy (Fig. 1).

The role of the pericarp and other seed covering struc-tures in limiting oxygen availability to the embryo (hypoxia) is another mechanism for coat-imposed dormancy (Benech-Arnold et al. 2006; Mendiondo et al. 2010; Dominguez et al. 2019). Comparative transcriptome and hormone analyses (IND, M$^-$, M$^+$) identified that up-regulated expression of hypoxia-responsive genes is a hall-mark of imbibed IND fruits (i.e. in M$^-$ seeds encased by the dead pericarp) as compared to M$^+$ seeds and bare M$^-$ seeds (Fig. 7). Identified hypoxia-responsive genes include the hypoxia-induced ERF-VII TF gene *AearERF71/73* and the fermentation genes *AearADH1a* and *AearPDC2*, but not *AearADH1b* and *AearPDC1*. While the *AearADH1a*, *AearPDC2*, and *AtPDC1* gene 5′-regulatory regions contain HRPE and putative ERF73 motifs, they do not contain G-box/ABRE motifs, whereas the *AearADH1b*, *AearPDC1*, and *AtADH1* genes do contain G-box/ABRE motifs. The rela-tive importance of AtERF71/73, ABA-related, and other TFs in the hypoxia-induced expression of the *AtADH1* gene is not completely resolved in *A. thaliana* (Lu et al. 1996; Kürsteiner et al. 2003; Gomez-Porras et al. 2007; Yang et al. 2011; Papdi et al. 2015; Gasch et al. 2016; Seok et al. 2022). Recent work with kiwifruit demonstrated that ERF73 and its target *cis*-elements involved in the hypoxia response seem to be conserved across the core Eudicots (Bai et al. 2021, 2024; Liu et al. 2022). For *Ae. arabicum*, we speculate that the observed duplication of the ADH genes, the differ-ences in the *cis*-regulatory motifs, the accumulation of *AearADH1a* and *AearPDC2* transcripts in M$^-$ seeds inside IND fruits, and pericarp-mediated hypoxia leading to PDC-ADH catalyzed ethanolic fermentation constitute a morph-specific adaptation that contributes to the increased dormancy of IND fruits.

Morphological and hormonal regulation: pericarp-ABA interactions as a key mechanism for distinct post-dispersal dimorphic diaspore responses to environmental cues

Earlier work with dormant barley grains and sunflower de-monstrated that hypoxia, imposed either artificially or by the maternal seed covering structures [barley (*Hordeum vul-gare*) glumellae, sunflower (*Helianthus annuus*) pericarp], in-terfered with ABA metabolism and increased embryo ABA

sensitivity (Benech-Arnold et al. 2006; Mendiondo et al. 2010; Andrade et al. 2015; Dominguez et al. 2019). In barley, this included transient ABA accumulation and ABI5 gene expression during dormancy maintenance. In sunflower, the pericarp-imposed dormancy was associated with increased embryo sensitivity to hypoxia and ABA, but with no change in embryo ABA content (Dominguez et al. 2019). As in *Ae. arabicum* pericarp (Fig. 6), sunflower pericarp also contained considerable amounts of ABA, SA, OPDA, JA, and JA-Ile (Andrade et al. 2015). In general, their contents declined during imbibition in both species, except ABA, which accumulated transiently in the sunflower pericarp, but declined in the dead pericarp of *Ae. arabicum*. The *Ae. arabicum* IND fruit versus M^- seed comparison revealed the decisive role of the pericarp and ABA in narrowing the germination-permissive window (Fig. 1). Using the three-way transcriptome and hormone comparison (IND, M^-, M^+), we could identify mechanisms not existing in monomorphic species. These include a very clear temperature-dependent up-regulation of ABA biosynthesis genes (including *AearNCED6*) and down-regulation of ABA 8′-hydroxylase genes (including *AearCYP707A3*) in M^- seeds within imbibed IND fruit morphs as compared to imbibed bare M^- seeds and the M^+ seed morphs (Fig. 5). At the 9 and 14 °C imbibition temperatures, the resultant ABA accumulation in M^- seeds inside IND fruits was especially elevated in the more dormant 20IND fruits as compared to in the less dormant 25IND fruits.

In agreement with a pericarp-enhanced ABA sensitivity of M^- embryos inside IND fruits, pericarp-enhanced expression of numerous ABA-related TFs including *AearAREB3*, *AearABI5*, *AearABF1*, and *AearGBF3* (Fig. 8) became evident during imbibition. Furthermoe, the presence of the pericarp affected the expression patterns for major ABA signaling genes, including for ABA receptors, PP2Cs, and SnRK2, which control the ABA-related TFs. The control of germinability by ABA signaling is, in part, achieved by regulating the expression of downstream cell wall remodeling genes (e.g. Finch-Savage and Leubner-Metzger 2006; Barrero et al. 2010; Shigeyama et al. 2016; Steinbrecher and Leubner-Metzger 2017, 2022; Holloway et al. 2021). Their expression in imbibed *Ae. arabicum* IND fruits, and M^+ and M^- seeds also exhibited pericarp- and temperature-dependent patterns (turquoise module in most cases), which is mainly mediated by hypoxia affecting ABA sensitivity and gene expression (Figs. 8 and 10).

The presented comprehensive molecular datasets on responses of dispersed dimorphic diaspores to ambient temperature, together with previous work on fruit/seed development (Lenser et al. 2018; Wilhelmsson et al. 2019; Arshad et al. 2021), highlights *Ae. arabicum* as the best experimental model system for heteromorphism so far. It provides a growing potential to understand developmental control and plasticity of fruit and seed dimorphism and its underpinning molecular, evolutionary, and ecological mechanisms as adaptation to environmental change. The comparative analysis of the M^+ seed morph, the IND fruit morph, and the bare M^- seed revealed morphological, hormonal, and

gene regulatory mechanisms of the pericarp-imposed dormancy. The dimorphic diaspores integrate parental and imbibition temperature differently, involving distinct transcriptional changes and ABA-related regulation. The *Ae. arabicum* web portal (https://plantcode.cup.uni-freiburg.de/aetar_db/index.php) with its genome DB and gene expression atlas comprises published transcriptome results (this work and Merai et al. 2019; Wilhelmsson et al. 2019; Arshad et al. 2021), is open for dataset additions, makes the data widely accessible, and provides a valuable source for future work on diaspore heteromorphism.

Materials and methods

Plant material, experimental growth conditions, and germination assays

Plants of the stone cress *Ae. arabicum* (L.) Andrz. ex DC. were grown from accession TUR ES1020 (from Turkey; Mohammadin et al. 2017, 2018; Merai et al. 2019), in Levington compost with added horticultural grade sand (F2 + S), under long-day conditions (16 h light/20 °C and 8 h dark/18 °C) in a glasshouse. Upon onset of flowering, plants were transferred to distinct PT regimes (20 versus 25 °C) during reproduction in otherwise identical growth chambers as described (Supplementary Fig. S1A). Mature M^+ seeds and IND fruits were harvested (Supplementary Table S1), further dried over silica gel for a week and either used immediately or stored at −20 °C in air-tight containers. For germination assays, dry mature seeds (M^+ or M^-) or IND fruits were placed in 3 cm Petri dishes containing two layers of filter paper, 3 ml distilled water, and 0.1% v/v plant preservative mixture (Plant Cell Technology). Temperature response profiles (Fig. 1C) were obtained by incubating plates on a GRD1-LH temperature gradient plate device (Grant Instruments Ltd., Cambridge, UK). Subsequent germination assays were conducted by incubating plates in MLR-350 Versatile Environmental Test Chambers (Sanyo-Panasonic) at the indicated imbibition temperature and 100 µmol s^{-1} m^{-2} continuous white light (Lenser et al. 2016). For germination assays under hypoxia conditions, compressed air (UN1002, BOC Ltd., Woking, UK) and oxygen-free nitrogen (BOC UN1066) were mixed to generate a $4.5 \pm 0.2\%$ oxygen atmosphere in hypoxia chambers (Stemcell Technolgies, Waterbeach, Cambridge, UK) with the plates (14 °C, continuous white light). Seed germination, scored as radicle emergence, of three biological replicates each with 20–25 seeds or fruits were analyzed.

MSI, biomechanical, and PE assays

MSI was performed with a VideometerLab (Mark4, Series 11, Videometer A/S, Denmark). Images were transformed using normalized canonical discriminant analysis to compare the two PTs. Biomechanical properties of the fruit coats were measured using a universal material testing machine (ZwickiLine Z0.5, Zwick Roell, Germany). Fruits were imbied

for 1 h before cutting them in half (fruit half covering the micropylar end of the seed and non-micropylar end of the seed) and re-dried overnight. Seeds were removed from the pericarps, and a metal probe with a diameter of 0.3 mm was driven into the sample at a speed of 2 mm/min while recording force and displacement. Tissue resistance was determined to be the maximal force from the force–displacement curve. PE was obtained as aqueous leachate by incubating ca. 0.5 g IND pericarp in 15 ml H_2O on a shaker for 2 h, followed by cleaning it using a 0.2 μm filter. Germination assays were conducted by comparing PE, H_2O (control), *cis*, *trans*-S(+)-ABA (ABA; Duchefa Biochemie, Haarlem, The Netherlands), SA (Alfa Aesar, Lancashire, UK), *cis*-(+)-12-OPDA (Cayman Chemical, MI, USA), (−)-JA (Cayman Chemical, MI, USA), or its isoleucine conjugate (JA-Ile; Cayman Chemical) at the concentrations indicated.

RNA-seq and RT-qPCR

Sampling of dry or imbibed M^+ seeds, M^- seeds, and IND fruits for molecular analyses was as described in the sampling scheme (Supplementary Fig. S1). Biological replicates of samples each corresponding to 20 mg dry weight of seed material were pulverized in liquid N_2 using mortar and pestle. Extraction of total RNA was performed as described by Graeber et al. (2011). RNA quantity and purity were determined using a NanoDrop spectrophotometer (ND-1000, ThermoScientific, Delaware, USA) and an Agilent 2100 Bioanalyzer with the RNA 6000 Nano Kit (Agilent Technologies, CA, USA) using the 2100 Expert Software to calculate RNA integrity number values. Four (RT-qPCR) or three (RNA-seq) biological replicates of RNA samples were used for downstream applications (sample naming scheme: Supplementary Table S2). Sequencing was performed at the Vienna BioCenter Core Facilities (VBCF) Next Generation Sequencing Unit, Vienna, Austria (www.vbcf.ac.at). RNA-seq libraries were sequenced in 50 bp single-end mode on Illumina HiSeq 2000 Analyzers using the manufacturer's standard module generation and sequencing protocols. The overall sequencing and mapping statistics for each library and the read counts are presented in Supplementary Data Set 1. RNA for RT-qPCR was extracted in an independent experiment using the RNAqueous Total RNA Isolation Kit with the addition of the Plant RNA Isolation Aid (Ambion, Thermo Fisher Scientific, Basingstoke, UK), followed by treatment with DNaseI (QIAGEN Ltd., Manchester, UK) and precipitation in 2 M LiCl. Precipitated RNA was washed in 70% v/v ethanol and resuspended in RNase-free water. RT-qPCR was conducted and analyzed as described (Graeber et al. 2011; Untergasser et al. 2012; Arshad et al. 2021) using primer sequences and reference genes listed in Supplementary Table S3.

Analyses of transcriptome data

Transcriptome assembly, data trimming, filtering, read mapping and feature counting, and DEG detection were performed as previously described (Wilhelmsson et al. 2019; Arshad et al. 2021). PCA was performed using the built-in R package "prcomp" (www.r-project.org) on $log(x + 1)$

transformed reads per kilobase per million (RPKM) values for 22,200 genes with non-zero values in at least one sample. Sample replicate RPKM values were averaged for 45 treatments and WGCNA (Zhang and Horvath 2005) implementation (Langfelder and Horvath 2008) in R was performed on $log_2(x + 1)$ transformed RPKM values for 11,260 genes whose average expression was >4 RPKM across all samples. The function blockwiseModules was used with default settings, other than to create a signed hybrid network distinguishing between positive and negative Pearson correlations using a soft power threshold of 24, minModuleSize of 50, mergeCutHeight of 0.25, and pamRespectsDendro set to False in single block. Module membership and significance for each gene were calculated (Pearson correlation with module eigengene; Supplementary Data Set 2). PCA analysis (Wickham 2016) for the 11,260 genes was performed as outlined above with transposed data. Module eigengene expression was correlated with sample traits using Pearson correlation. GO term enrichment in module gene lists was calculated using the R package topGO (Alexa and Rahnenfuhrer 2023) using the elim or classic method with Fisher's exact test. Geneious 8.1.9 (https://www.geneious.com) was used to visualize motif positions. Gene identifier and symbols (Supplementary Table S2) are according to earlier publications of the *Ae. arabicum* genome and transcriptome (Haudry et al. 2013; Merai et al. 2019; Nguyen et al. 2019; Wilhelmsson et al. 2019; Arshad et al. 2021) and the *Ae. arabicum* web portal (https://plantcode.cup.uni-freiburg.de/aetar_db/index.php) links this to the current (Fernandez-Pozo et al. 2021) and future genome DB and gene expression atlas.

Gene promoter analyses

Promoter motif enrichment in the start codon −1,000 to +100 bp region was analyzed using the Analysis of Motif Enrichment tool (McLeay and Bailey 2010) using MEME Suite (https://meme-suite.org/; Bailey et al. 2015) to identify enrichment of motifs from the ArabidopsisDAPv1 DB (O'Malley et al. 2016). Input sequences (module gene list) were compared to control sequences (all promoter sequences) using average odds score, Fisher's exact test, fractional score threshold of 0.25, E-value cutoff of 10, and 0-order background model. FIMO (Grant et al. 2011) on MEME Suite was used to scan sequences for chosen motifs. Chord diagram was drawn using R package "circlize" (Gu et al. 2014).

Phytohormone quantification

For quantification of jasmonates (JA, JA-Ile, and *cis*-OPDA), auxins (IAA and its catabolite oxIAA), abscisates (ABA, PA, and DPA), and SA, internal standards, containing 20 pmol of $[^2H_4]$SA and $[^2H_5]$OPDA, 10 pmol each of $[^2H_6]$ABA, $[^2H_6]$JA, and $[^2H_2]$JA-Ile, and 5 pmol each of $[^2H_3]$PA, $[^2H_3]$DPA, $[^{13}C_6]$IAA, and $[^{13}C_6]$oxIAA (all from Olchemim Ltd, Czech Republic), and 1 ml of ice-cold methanol:water (10:90, v/v) were added to 10 mg of freeze-dried and homogenized samples. Sample mixtures were homogenized using an MM400

vibration mill for 5 min at 27 Hz (Retsch Technology GmbH, Germany), sonicated for 3 min at 4 °C using an ultrasonic bath, and then extracted for 30 min (15 rpm) at 4 °C using a rotary disk shaker. Samples were centrifuged at 20,000 rpm (15 min, 4 °C), the supernatant purified using pre-equilibrated Oasis Hydrophilic-Lipophilic-Balanced (HLB) cartridges (1 cc, 30 mg, Waters), and evaporated to dryness under nitrogen (30 °C; Flokova et al. 2014). The evaporated samples were reconstituted in 40 µl of the mobile phase (15% acetonitrile, v/v) and analyzed by ultrahigh performance liquid chromatography-electrospray ionization tandem mass spectrometry (UHPLC-ESI-MS/MS) as described by Šimura et al. (2018). All phytohormones were detected using a multiple-reaction monitoring mode of the transition of the precursor ion to the appropriate product ion. Masslynx 4.1 software (Waters, Milford, MA, USA) was used to analyze the data, and the standard isotope dilution method (Rittenberg and Foster 1940) was used to quantify the phytohormone levels. Five independent biological replicates were performed.

Statistical analysis

Germination data were evaluated by comparing final germination percentage (G_{max}) and germination rate (speed). Germination curve fits and $T_{50\%}$ were calculated with GERMINATOR (Joosen et al. 2010). An unpaired *t*-test was used to compare the mean values for tissue resistance (biomechanical analysis of pericarp) of the two PTs. All statistical analyses were performed in GraphPad Prism (v. 8.01, GraphPad Software Inc., San Diego, CA, USA). Statistical data are provided in Supplementary Table S4.

Accession numbers

The RNA-seq data discussed in this publication have been deposited at the National Library of Medicine (NCBI) SRA, BioProjects PRJNA611900 (dry seed) and PRJNA639669 (imbibed seed), accessible at https://www.ncbi.nlm.nih.gov/sra; metadata about the samples are also available as part of this publication (Supplementary Data Set 1).

Author contributions

K.G., K.M., G.T., M.S., O.M.S., M.E.S., O.N., S.A.R., and G.L.-M. conceived the project and conceptualized the work. J.O.C., P.K.I.W., and K.G. performed the majority of experiments; K.G., Z.M., and J.O.C. prepared and handled samples; J.O.C., P.K.I.W., K.K.U., W.A., S.A.R., and G.L.-M. performed the transcriptomics data analysis. J.O.C., T.S., and M.P. performed RT-qPCR and hypoxia analyses. J.O.C., T.S., and M.P. performed germination, biomechanical experiments, and MSI analyses. N.F.-P., J.O.C., and S.A.R. developed and implemented the gene expression atlas. T.-P.N., K.G., W.A., K.M., and M.E.S. conducted the environmental simulation experiment and generated the plant material. I.P., D.T., O.N., and M.S. performed the hormone analysis. J.O.C. and G.L.-M. wrote the manuscript. All authors read and commented on the manuscript.

Supplementary data

The following materials are available in the online version of this article.

Supplementary Figure S1. Large-scale diaspore production experiment and sampling.

Supplementary Figure S2. *Aethionema arabicum* gene expression atlas.

Supplementary Figure S3. PCA of transcriptome data (RNA-seq).

Supplementary Figure S4. Expression of WGCNA modules.

Supplementary Figure S5. Temperature responses and ABA and GA metabolism.

Supplementary Figure S6. Hormone contents in response to temperatures.

Supplementary Figure S7. Effects of PE on germination and gene expression.

Supplementary Figure S8. Pericarp (fruit coat) biomechanics.

Supplementary Figure S9. TFs and promoter motifs of fermentation genes.

Supplementary Figure S10. Transcript abundance patterns of the seed-specific Perl's pathway.

Supplementary Figure S11. Transcript abundance patterns of hypoxia-regulated genes.

Supplementary Figure S12. RT-qPCR analysis of hypoxia and ABA effects.

Supplementary Figure S13. Detail comparison of fermentation gene promoters.

Supplementary Figure S14. Transcript abundance patterns of ABA-related genes.

Supplementary Figure S15. Transcript abundance patterns of transcription/translation genes.

Supplementary Figure S16. Transcript abundance patterns of cell wall remodeling genes.

Supplementary Table S1. *Aethionema arabicum* seed and fruit harvest results.

Supplementary Table S2. *Aethionema arabicum* gene IDs, symbols, and modules.

Supplementary Table S3. RT-qPCR primers used.

Supplementary Table S4. Statistical data.

Supplementary Data Set 1. Gene annotations, DEGs, RPKM values, raw counts, and Sequencing Read Archive (SRA) accessions.

Supplementary Data Set 2. WGCNA modules and GO term enrichment analysis.

Supplementary Data Set 3. Promoter Analysis of Motif Enrichment (AME) and chord diagram data.

Supplementary Data Set 4. Promoter motif scanning by Find Individual Motif Occurrences (FIMO).

Funding

Data availability

The normalized transcriptome data from this study and associated previous studies (Merai et al. 2019; Wilhelmsson et al. 2019; Arshad et al. 2021) can be accessed and visualized at the *Ae. arabicum* web portal (https://plantcode.cup.uni-freiburg.de/aetar_db/index.php). For *Ae. arabicum* gene IDs, see Supplementary Figs. S15 and S16 and Table S2, or the Expression Atlas (https://plantcode.cup.uni-freiburg.de/aetar_db/index.php); for RNA-seq single values, see the Expression Atlas or Supplementary Data Set 1. All other data presented or analyzed in this published article are available online through the supplements.

References

Alexa A, Rahnenfuhrer J. topGO: enrichment analysis for gene ontology. R package version 2.52.0; 2023. https://doi.org/10.18129/B9.bioc.topGO.

Andrade A, Riera N, Lindstrom L, Alemano S, Alvarez D, Abdala G, Vigliocco A. Pericarp anatomy and hormone profiles of cypselas in dormant and non-dormant inbred sunflower lines. Plant Biol. 2015:**17**(2):351–360. https://doi.org/10.1111/plb.12244

Arshad W, Lenser T, Wilhelmsson PKI, Chandler JO, Steinbrecher T, Marone F, Pérez M, Collinson ME, Stuppy W, Rensing SA, et al. A tale of two morphs: developmental patterns and mechanisms of seed coat differentiation in the dimorphic diaspore model *Aethionema arabicum* (Brassicaceae). Plant J. 2021:**107**(1):166–181. https://doi.org/10.1111/tpj.15283

Arshad W, Marone F, Collinson ME, Leubner-Metzger G, Steinbrecher T. Fracture of the dimorphic fruits of *Aethionema arabicum* (Brassicaceae). Botany. 2020:**98**(1):65–75. https://doi.org/10.1139/cjb-2019-0014

Arshad W, Sperber K, Steinbrecher T, Nichols B, Jansen VAA, Leubner-Metzger G, Mummenhoff K. Dispersal biophysics and adaptive significance of dimorphic diaspores in the annual *Aethionema arabicum* (Brassicaceae). New Phytol. 2019:**221**(3):1434–1446. https://doi.org/10.1111/nph.15490

Bai D, Zhong Y, Gu S, Qi X, Sun L, Lin M, Wang R, Li Y, Hu C, Fang J. AvERF73 positively regulates waterlogging tolerance in kiwifruit by participating in hypoxia response and mevalonate pathway. Hortic Plant J. https://doi.org/10.1016/j.hpj.2023.05.021. 2024, preprint: not peer reviewed.

Bai D-F, Li Z, Hu C-G, Zhang Y-J, Muhammad A, Zhong Y-P, Fang J-B. Transcriptome-wide identification and expression analysis of *ERF* family genes in *Actinidia valvata* during waterlogging stress. Sci Hortic-Amsterdam. 2021:**281**:109994. https://doi.org/10.1016/j.scienta.2021.109994

Bailey TL, Johnson J, Grant CE, Noble WS. The MEME suite. Nucl Acids Res. 2015:**43**(W1):W39–W49. https://doi.org/10.1093/nar/gkv416

Barrero JM, Millar AA, Griffiths J, Czechowski T, Scheible WR, Udvardi M, Reid JB, Ross JJ, Jacobsen JV, Gubler F. Gene expression profiling identifies two regulatory genes controlling dormancy and ABA sensitivity in *Arabidopsis* seeds. Plant J. 2010:**61**(4):611–622. https://doi.org/10.1111/j.1365-313X.2009.04088.x

Baskin JM, Lu JJ, Baskin CC, Tan DY, Wang L. Diaspore dispersal ability and degree of dormancy in heteromorphic species of cold deserts of Northwest China: a review. Perspect Plant Ecol Evol Syst. 2014:**16**(2):93–99. https://doi.org/10.1016/j.ppees.2014.02.004

Batlla D, Malavert C, Farnocchia RBF, Footitt S, Benech-Arnold RL, Finch-Savage WE. A quantitative analysis of temperature-dependent seasonal dormancy cycling in buried *Arabidopsis thaliana* seeds can predict seedling emergence in a global warming scenario. J Exp Bot. 2022:**73**(8):2454–2468. https://doi.org/10.1093/jxb/erac038

Benech-Arnold RL, Gualano N, Leymarie J, Come D, Corbineau F. Hypoxia interferes with ABA metabolism and increases ABA sensitivity in embryos of dormant barley grains. J Exp Bot. 2006:**57**(6):1423–1430. https://doi.org/10.1093/jxb/erj122

Bhattacharya S, Sperber K, Ozudogru B, Leubner-Metzger G, Mummenhoff K. Naturally-primed life strategy plasticity of dimorphic *Aethionema arabicum* facilitates optimal habitat colonization. Sci Rep. 2019:**9**(1):16108. https://doi.org/10.1038/s41598-019-52520-y

Borisjuk L, Rolletschek H. The oxygen status of the developing seed. New Phytol. 2009:**182**(1):17–30. https://doi.org/10.1111/j.1469-8137.2008.02752.x

Bueso E, Munoz-Bertomeu J, Campos F, Brunaud V, Martinez L, Sayas E, Ballester P, Yenush L, Serrano R. *Arabidopsis thaliana* HOMEOBOX25 uncovers a role for gibberellins in seed longevity. Plant Physiol. 2014:**164**(2):999–1010. https://doi.org/10.1104/pp.113.232223

Cadman CSC, Toorop PE, Hilhorst HWM, Finch-Savage WE. Gene expression profiles of Arabidopsis cvi seed during cycling through dormant and non-dormant states indicate a common underlying dormancy control mechanism. Plant J. 2006:**46**(5):805–822. https://doi.org/10.1111/j.1365-313X.2006.02738.x

Christianson JA, Wilson IW, Llewellyn DJ, Dennis ES. The low-oxygen induced NAC domain transcription factor ANAC102 affects viability of *Arabidopsis thaliana* seeds following low-oxygen treatment. Plant Physiol. 2009:**149**(4):1724–1738. https://doi.org/10.1104/pp.108.131912

Corbineau F. Oxygen, a key signalling factor in the control of seed germination and dormancy. Seed Sci Res. 2022:**32**(3):126–136. https://doi.org/10.1017/S096025852200006X

Dave A, Vaistij FE, Gilday AD, Penfield SD, Graham IA. Regulation of *Arabidopsis thaliana* seed dormancy and germination by 12-oxo-

phytodienoic acid. J Exp Bot. 2016:**67**(8):2277–2284. https://doi.org/10.1093/jxb/erw028

Dominguez CP, Rodriguez MV, Batlla D, de Salamone IEG, Mantese AI, Andreani AL, Benech-Arnold RL. Sensitivity to hypoxia and microbial activity are instrumental in pericarp-imposed dormancy expression in sunflower (*Helianthus annuus* L.). Seed Sci Res. 2019:**29**(2):85–96. https://doi.org/10.1017/S0960258519000060

Donohue K, Rubio de Casas R, Burghardt L, Kovach K, Willis CG. Germination, postgermination adaptation, and species ecological ranges. Annu Rev Ecol Evol Syst. 2010:**41**:293–319. https://doi.org/10.1146/annurev-ecolsys-102209-144715

Fernandez-Pascual E, Mattana E, Pritchard HW. Seeds of future past: climate change and the thermal memory of plant reproductive traits. Biol Rev Camb Philos Soc. 2019:**94**(2):439–456. https://doi.org/10.1111/brv.12461

Fernandez-Pozo N, Bombarely A. EasyGDB: a low-maintenance and highly customizable system to develop genomics portals. Bioinformatics (Oxford, England). 2022:**38**(16):4048–4050. https://doi.org/10.1093/bioinformatics/btac412

Fernandez-Pozo N, Metz T, Chandler JO, Gramzow L, Merai Z, Maumus F, Scheid OM, Theissen G, Schranz ME, Leubner-Metzger G, et al. *Aethionema arabicum* genome annotation using PacBio full-length transcripts provides a valuable resource for seed dormancy and Brassicaceae evolution research. Plant J. 2021:**106**(1):275–293. https://doi.org/10.1111/tpj.15161

Finch-Savage WE, Footitt S. Seed dormancy cycling and the regulation of dormancy mechanisms to time germination in variable field environments. J Exp Bot. 2017:**68**(4):843–856. https://doi.org/10.1093/jxb/erw477

Finch-Savage WE, Leubner-Metzger G. Seed dormancy and the control of germination. New Phytol. 2006:**171**(3):501–523. https://doi.org/10.1111/j.1469-8137.2006.01787.x

Flokova K, Tarkowska D, Miersch O, Strnad M, Wasternack C, Novak O. UHPLC-MS/MS based target profiling of stress-induced phytohormones. Phytochemistry. 2014:**105**:147–157. https://doi.org/10.1016/j.phytochem.2014.05.015

Footitt S, Walley PG, Lynn JR, Hambidge AJ, Penfield S, Finch-Savage WE. Trait analysis reveals DOG1 determines initial depth of seed dormancy, but not changes during dormancy cycling that result in seedling emergence timing. New Phytol. 2020:**225**(5):2035–2047. https://doi.org/10.1111/nph.16081

Gasch P, Fundinger M, Muller JT, Lee T, Bailey-Serres J, Mustroph A. Redundant ERF-VII transcription factors bind to an evolutionarily conserved *cis*-motif to regulate hypoxia-responsive gene expression in Arabidopsis. Plant Cell. 2016:**28**(1):160–180. https://doi.org/10.1105/tpc.15.00866

Gianella M, Bradford KJ, Guzzon F. Ecological, (epi)genetic and physiological aspects of bet-hedging in angiosperms. Plant Reprod. 2021:**34**(1):21–36. https://doi.org/10.1007/s00497-020-00402-z

Gibbs DJ, Lee SC, Md Isa N, Gramuglia S, Fukao T, Bassel GW, Correia CS, Corbineau F, Theodoulou FL, Bailey-Serres J, et al. Homeostatic response to hypoxia is regulated by the N-end rule pathway in plants. Nature. 2011:**479**(7373):415–419. https://doi.org/10.1038/nature10534

Gomez-Porras JL, Riano-Pachon DM, Dreyer I, Mayer JE, Mueller-Roeber B. Genome-wide analysis of ABA-responsive elements ABRE and CE3 reveals divergent patterns in Arabidopsis and rice. BMC Genomics. 2007:**8**:260. https://doi.org/10.1186/1471-2164-8-260

Graeber K, Linkies A, Steinbrecher T, Mummenhoff K, Tarkowská D, Turečková V, Ignatz M, Sperber K, Voegele A, de Jong H, et al. *DELAY OF GERMINATION 1* mediates a conserved coat dormancy mechanism for the temperature- and gibberellin-dependent control of seed germination. Proc Natl Acad Sci U S A. 2014:**111**(34): E3571–E3580. https://doi.org/10.1073/pnas.1403851111

Graeber K, Linkies A, Wood ATA, Leubner-Metzger G. A guideline to family-wide comparative state-of-the-art quantitative RT-PCR analysis exemplified with a Brassicaceae cross-species seed germination case study. Plant Cell. 2011:**23**(6):2045–2063. https://doi.org/10.1105/tpc.111.084103

Grafi G. Dead but not dead end: multifunctional role of dead organs enclosing embryos in seed biology. Int J Mol Sci. 2020:**21**(21):8024. https://doi.org/10.3390/ijms21218024

Grant CE, Bailey TL, Noble WS. FIMO: scanning for occurrences of a given motif. Bioinformatics (Oxford, England). 2011:**27**(7):1017–1018. https://doi.org/10.1093/bioinformatics/btr064

Gu ZG, Gu L, Eils R, Schlesner M, Brors B. Circlize implements and enhances circular visualization in R. Bioinformatics (Oxford, England). 2014:**30**(19):2811–2812. https://doi.org/10.1093/bioinformatics/btu393

Hall JC, Tisdale TE, Donohue K, Kramer EM. Developmental basis of an anatomical novelty: heteroarthrocarpy in *Cakile lanceolata* and *Erucaria erucarioides* (Brassicaceae). Int J Plant Sci. 2006:**167**(4): 771–789. https://doi.org/10.1086/504928

Haudry A, Platts AE, Vello E, Hoen DR, Leclercq M, Williamson RJ, Forczek E, Joly-Lopez Z, Steffen JG, Hazzouri KM, et al. An atlas of over 90,000 conserved noncoding sequences provides insight into crucifer regulatory regions. Nat Genet. 2013:**45**(8):891–898. https://doi.org/10.1038/ng.2684

Hoang HH, Bailly C, Corbineau F, Leymarie J. Induction of secondary dormancy by hypoxia in barley grains and its hormonal regulation. J Exp Bot. 2013:**64**(7):2017–2025. https://doi.org/10.1093/jxb/ert062

Holloway T, Steinbrecher T, Pérez M, Seville A, Stock D, Nakabayashi K, Leubner-Metzger G. Coleorhiza-enforced seed dormancy: a novel mechanism to control germination in grasses. New Phytol. 2021:**229**(4):2179–2191. https://doi.org/10.1111/nph.16948

Ignatz M, Hourston JE, Tureckova V, Strnad M, Meinhard J, Fischer U, Steinbrecher T, Leubner-Metzger G. The biochemistry underpinning industrial seed technology and mechanical processing of sugar beet. Planta. 2019:**250**(5):1717–1729. https://doi.org/10.1007/s00425-019-03257-5

Imbert E. Ecological consequences and ontogeny of seed heteromorphism. Perspect Plant Ecol Evol Syst. 2002:**5**(1):13–36. https://doi.org/10.1078/1433-8319-00021

Iwasaki M, Penfield S, Lopez-Molina L. Parental and environmental control of seed dormancy in *Arabidopsis thaliana*. Annu Rev Plant Biol. 2022:**73**:355–378. https://doi.org/10.1146/annurev-arplant-102820-090750

Joosen RVL, Kodde J, Willems LAJ, Ligterink W, van der Plas LHW, Hilhorst HWM. GERMINATOR: a software package for high-throughput scoring and curve fitting of *Arabidopsis* seed germination. Plant J. 2010:**62**(1):148–159. https://doi.org/10.1111/j.1365-313X.2009.04116.x

Ju L, Jing YX, Shi PT, Liu J, Chen JS, Yan JJ, Chu JF, Chen K-M, Sun JQ. JAZ proteins modulate seed germination through interaction with ABI5 in bread wheat and Arabidopsis. New Phytol. 2019:**223**(1): 246–260. https://doi.org/10.1111/nph.15757

Khadka J, Raviv B, Swetha B, Grandhi R, Singiri JR, Novoplansky N, Gutterman Y, Galis I, Huang ZY, Grafi G. Maternal environment alters dead pericarp biochemical properties of the desert annual plant *Anastatica hierochuntica* L. PLoS One. 2020:**15**(7):e0237045. https://doi.org/10.1371/journal.pone.0237045

Kürsteiner O, Dupuis I, Kuhlemeier C. The pyruvate decarboxylase1 gene of Arabidopsis is required during anoxia but not other environmental stresses. Plant Physiol. 2003:**132**(2):968–978. https://doi.org/10.1104/pp.102.016907

Langfelder P, Horvath S. WGCNA: an R package for weighted correlation network analysis. BMC Bioinformatics. 2008:**9**:559. https://doi.org/10.1186/1471-2105-9-559

Lee TA, Bailey-Serres J. Conserved and nuanced hierarchy of gene regulatory response to hypoxia. New Phytol. 2021:**229**(1):71–78. https://doi.org/10.1111/nph.16437

Lenser T, Graeber K, Cevik OS, Adiguzel N, Donmez AA, Grosche C, Kettermann M, Mayland-Quellhorst S, Merai Z, Mohammadin S, et al. Developmental control and plasticity of fruit and seed

dimorphism in *Aethionema arabicum*. Plant Physiol. 2016:**172**(3): 1691–1707. https://doi.org/10.1104/pp.16.00838

Lenser T, Tarkowska D, Novak O, Wilhelmsson PKI, Bennett T, Rensing SA, Strnad M, Theissen G. When the BRANCHED network bears fruit: how carpic dominance causes fruit dimorphism in *Aethionema*. Plant J. 2018:**94**(2):352–371. https://doi.org/10.1111/tpj.13861

Linkies A, Leubner-Metzger G. Beyond gibberellins and abscisic acid: how ethylene and jasmonates control seed germination. Plant Cell Rep. 2012:**31**(2):253–270. https://doi.org/10.1007/s00299-011-1180-1

Liu J, Chen Y, Wang W-Q, Liu J-H, Zhu C-Q, Zhong Y-P, Zhang H-Q, Liu X-F, Yin X-R. Transcription factors AcERF74/75 respond to waterlogging stress and trigger alcoholic fermentation-related genes in kiwifruit. Plant Sci. 2022:**314**:111115. https://doi.org/10.1016/j.plantsci.2021.111115

Liu R, Wang L, Tanveer M, Song J. Seed heteromorphism: an important adaptation of halophytes for habitat heterogeneity. Front Plant Sci. 2018:**9**:1515. https://doi.org/10.3389/fpls.2018.01515

Loades E, Perez M, Tureckova V, Tarkowska D, Strnad M, Seville A, Nakabayashi K, Leubner-Metzger G. Distinct hormonal and morphological control of dormancy and germination in *Chenopodium album* dimorphic seeds. Front Plant Sci. 2023:**14**:1156794. https://doi.org/10.3389/fpls.2023.1156794

Lu GH, Paul AL, McCarty DR, Ferl RJ. Transcription factor veracity: is GBF3 responsible for ABA-regulated expression of Arabidopsis *Adh*? Plant Cell. 1996:**8**(5):847–857. https://doi.org/10.1105/tpc.8.5.847

Lu JJ, Tan DY, Baskin JM, Baskin CC. Post-release fates of seeds in dehiscent and indehiscent siliques of the diaspore heteromorphic species *Diptychocarpus strictus* (Brassicaceae). Perspect Plant Ecol Evol Syst. 2015a:**17**(4):255–262. https://doi.org/10.1016/j.ppees.2015.04.001

Lu JJ, Tan DY, Baskin CC, Baskin JM. Role of indehiscent pericarp in formation of soil seed bank in five cold desert Brassicaceae species. Plant Ecol. 2017a:**218**(10):1187–1200. https://doi.org/10.1007/s11258-017-0760-8

Lu JJ, Tan DY, Baskin CC, Baskin JM. Delayed dehiscence of the pericarp: role in germination and retention of viability of seeds of two cold desert annual Brassicaceae species. Plant Biol (Stuttg). 2017b: **19**(1):14–22. https://doi.org/10.1111/plb.12457

Lu JJ, Zhou YM, Tan DY, Baskin CC, Baskin JM. Seed dormancy in six cold desert Brassicaceae species with indehiscent fruits. Seed Sci Res. 2015b:**25**(3):276–285. https://doi.org/10.1017/S0960258515000215

Mamut J, Tan D-Y, Baskin CC, Baskin JM. Role of trichomes and pericarp in the seed biology of the desert annual *Lachnoloma lehmannii* (Brassicaceae). Ecol Res. 2014:**29**(1):33–44. https://doi.org/10.1007/s11284-013-1098-x

McLeay RC, Bailey TL. Motif enrichment analysis: a unified framework and an evaluation on ChIP data. BMC Bioinformatics. 2010:**11**:165. https://doi.org/10.1186/1471-2105-11-165

Mendiondo GM, Leymarie J, Farrant JM, Corbineau F, Benech-Arnold RL. Differential expression of abscisic acid metabolism and signalling genes induced by seed-covering structures or hypoxia in barley (*Hordeum vulgare* L.) grains. Seed Sci Res. 2010:**20**(2): 69–77. https://doi.org/10.1017/S0960258509990262

Merai Z, Graeber K, Wilhelmsson P, Ullrich KK, Arshad W, Grosche C, Tarkowska D, Tureckova V, Strnad M, Rensing SA, et al. *Aethionema arabicum*: a novel model plant to study the light control of seed germination. J Exp Bot. 2019:**70**(12):3313–3328. https://doi.org/10.1093/jxb/erz146

Merai Z, Xu F, Musilek A, Ackerl F, Khalil S, Soto-Jimenez LM, Lalatovic K, Klose C, Tarkowska D, Tureckova V, et al. Phytochromes mediate germination inhibition under red, far-red, and white light in *Aethionema arabicum*. Plant Physiol. 2023:**192**(2): 1584–1602. https://doi.org/10.1093/plphys/kiad138

Mohammadin S, Peterse K, van de Kerke SJ, Chatrou LW, Donmez AA, Mummenhoff K, Pires JC, Edger PP, Al-Shehbaz IA, Schranz ME. Anatolian origins and diversification of *Aethionema*, the sister lineage of the core Brassicaceae. Am J Bot. 2017:**104**(7):1042–1054. https://doi.org/10.3732/ajb.1700091

Mohammadin S, Wang W, Liu T, Moazzeni H, Ertugrul K, Uysal T, Christodoulou CS, Edger PP, Pires JC, Wright SI, et al. Genome-wide nucleotide diversity and associations with geography, ploidy level and glucosinolate profiles in *Aethionema arabicum* (Brassicaceae). Plant Syst Evol. 2018:**304**(5):619–630. https://doi.org/10.1007/s00606-018-1494-3

Mohammed S, Turckova V, Tarkowska D, Strnad M, Mummenhoff K, Leubner-Metzger G. Pericarp-mediated chemical dormancy controls the fruit germination of the invasive hoary cress (*Lepidium draba*), but not of hairy whitetop (*Lepidium appelianum*). Weed Sci. 2019:**67**(5):560–571. https://doi.org/10.1017/wsc.2019.33

Mühlhausen A, Lenser T, Mummenhoff K, Theissen G. Evidence that an evolutionary transition from dehiscent to indehiscent fruits in *Lepidium* (Brassicaceae) was caused by a change in the control of valve margin identity genes. Plant J. 2013:**73**(5):824–835. https://doi.org/10.1111/tpj.12079

Nambara E, Okamoto M, Tatematsu K, Yano R, Seo M, Kamiya Y. Abscisic acid and the control of seed dormany and germination. Seed Sci Res. 2010:**20**(2):55–67. https://doi.org/10.1017/S0960258510000012

Nguyen TP, Muhlich C, Mohammadin S, van den Bergh E, Platts AE, Haas FB, Rensing SA, Schranz ME. Genome improvement and genetic map construction for *Aethionema arabicum*, the first divergent branch in the Brassicaceae family. G3 (Bethesda). 2019:**9**(11): 3521–3530. https://doi.org/10.1534/g3.119.400657

Nichols BS, Leubner-Metzger G, Jansen VAA. Between a rock and a hard place: adaptive sensing and site-specific dispersal. Ecol Lett. 2020:**23**(9):1370–1379. https://doi.org/10.1111/ele.13564

O'Malley RC, Huang SSC, Song L, Lewsey MG, Bartlett A, Nery JR, Galli M, Gallavotti A, Ecker JR. Cistrome and epicistrome features shape the regulatory DNA landscape. Cell. 2016:**165**(5):1280–1292. https://doi.org/10.1016/j.cell.2016.04.038

Papdi C, Perez-Salamo I, Joseph MP, Giuntoli B, Bogre L, Koncz C, Szabados L. The low oxygen, oxidative and osmotic stress responses synergistically act through the ethylene response factor VII genes RAP2.12, RAP2.2 and RAP2.3. Plant J. 2015:**82**(5):772–784. https://doi.org/10.1111/tpj.12848

Penfield S, MacGregor DR. Effects of environmental variation during seed production on seed dormancy and germination. J Exp Bot. 2017:**68**(4):819–825. https://doi.org/10.1093/jxb/erw436

Renard J, Martinez-Almonacid I, Castillo IQ, Sonntag A, Hashim A, Bissoli G, Campos L, Munoz-Bertomeu J, Ninoles R, Roach T, et al. Apoplastic lipid barriers regulated by conserved homeobox transcription factors extend seed longevity in multiple plant species. New Phytol. 2021:**231**(2):679–694. https://doi.org/10.1111/nph.17399

Reynoso MA, Kajala K, Bajic M, West DA, Pauluzzi G, Yao AI, Hatch K, Zumstein K, Woodhouse M, Rodriguez-Medina J, et al. Evolutionary flexibility in flooding response circuitry in angiosperms. Science. 2019:**365**(6459):1291–1295. https://doi.org/10.1126/science.aax8862

Rittenberg D, Foster GL. A new procedure for quantitative analysis by isotope dilution, with application to the determination of amino acids and fatty acids. J Biol Chem. 1940:**133**(3):737–744. https://doi.org/10.1016/S0021-9258(18)73304-8

Scheler C, Weitbrecht K, Pearce SP, Hampstead A, Buettner-Mainik A, Lee KJD, Voegele A, Oracz K, Dekkers BJW, Wang X, et al. Promotion of testa rupture during garden cress germination involves seed compartment-specific expression and activity of pectin methylesterases. Plant Physiol. 2015:**167**(1):200–215. https://doi.org/10.1104/pp.114.247429

Seok H-Y, Tran HT, Lee S-Y, Moon Y-H. *AtERF71/HRE2*, an Arabidopsis AP2/ERF transcription factor gene, contains both positive and negative *cis*-regulatory elements in is promoter region involved in hypoxia and salt stress responses. Int J Mol Sci. 2022:**23**(10):5310. https://doi.org/10.3390/ijms23105310

Shigeyama T, Watanabe A, Tokuchi K, Toh S, Sakurai N, Shibuya N, Kawakami N. α-Xylosidase plays essential roles in xyloglucan remodelling, maintenance of cell wall integrity, and seed germination in *Arabidopsis thaliana*. J Exp Bot. 2016:**67**(19):5615–5629. https://doi.org/10.1093/jxb/erw321

Silva AT, Ribone PA, Chan RL, Ligterink W, Hilhorst HWM. A predictive coexpression network identifies novel genes controlling the seed-to-seedling phase transition in *Arabidopsis thaliana*. Plant Physiol. 2016:**170**(4):2218–2231. https://doi.org/10.1104/pp.15.01704

Šimura J, Antoniadi I, Siroka J, Tarkowská D, Strnad M, Ljung K, Novak O. Plant hormonomics: multiple phytohormone profiling by targeted metabolomics. Plant Physiol. 2018:**177**(2):476–489. https://doi.org/10.1104/pp.18.00293

Sperber K, Steinbrecher T, Graeber K, Scherer G, Clausing S, Wiegand N, Hourston JE, Kurre R, Leubner-Metzger G, Mummenhoff K. Fruit fracture biomechanics and the release of *Lepidium didymum* pericarp-imposed mechanical dormancy by fungi. Nat Commun. 2017:**8**(1):1868. https://doi.org/10.1038/s41467-017-02051-9

Stamm P, Topham AT, Mukhtar NK, Jackson MDB, Tome DFA, Beynon JL, Bassel GW. The transcription factor ATHB5 affects GA-mediated plasticity in hypocotyl cell growth during seed germination. Plant Physiol. 2017:**173**(1):907–917. https://doi.org/10.1104/pp.16.01099

Steinbrecher T, Leubner-Metzger G. The biomechanics of seed germination. J Exp Bot. 2017:**68**(4):765–783. https://doi.org/10.1093/jxb/erw428

Steinbrecher T, Leubner-Metzger G. Xyloglucan remodelling enzymes and the mechanics of plant seed and fruit biology. J Exp Bot. 2022:**73**(5):1253–1257. https://doi.org/10.1093/jxb/erac020

Takeno K, Yamaguchi H. Diversity in seed-germination behavior in relation to heterocarpy in *Salsola komarovii* iljin. Bot Mag Tokyo. 1991:**104**(3):207–215. https://doi.org/10.1007/BF02489453

Untergasser A, Cutcutache I, Koressaar T, Ye J, Faircloth BC, Remm M, Rozen SG. Primer3—new capabilities and interfaces. Nucl Acids Res. 2012:**40**(15):e115. https://doi.org/10.1093/nar/gks596

van Veen H, Akman M, Jamar DC, Vreugdenhil D, Kooiker M, van Tienderen P, Voesenek LA, Schranz ME, Sasidharan R. Group VII ethylene response factor diversification and regulation in four species from flood-prone environments. Plant Cell Environ. 2014:**37**(10):2421–2432. https://doi.org/10.1111/pce.12302

Walck JL, Hidayati SN, Dixon KW, Thompson K, Poschlod P. Climate change and plant regeneration from seed. Global Change Biol. 2011:**17**(6):2145–2161. https://doi.org/10.1111/j.1365-2486.2010.02368.x

Wang L, Hua DP, He JN, Duan Y, Chen ZZ, Hong XH, Gong ZZ. Auxin response factor2 (ARF2) and its regulated homeodomain gene HB33 mediate abscisic acid response in Arabidopsis. PLoS Genet. 2011:**7**(7):e1002172. https://doi.org/10.1371/journal.pgen.1002172

Weitbrecht K, Müller K, Leubner-Metzger G. First off the mark: early seed germination. J Exp Bot. 2011:**62**(10):3289–3309. https://doi.org/10.1093/jxb/err030

Wickham H. Ggplot2: elegant graphics for data analysis. New York: Springer-Verlag; 2016.

Wilhelmsson PKI, Chandler JO, Fernandez-Pozo N, Graeber K, Ullrich KK, Arshad W, Khan S, Hofberger J, Buchta K, Edger PP, et al. Usability of reference-free transcriptome assemblies for detection of differential expression: a case study on *Aethionema arabicum* dimorphic seeds. BMC Genomics. 2019:**20**(1):95. https://doi.org/10.1186/s12864-019-5452-4

Yang C-Y, Hsu F-C, Li J-P, Wang N-N, Shih M-C. The AP2/ERF transcription factor AtERF73/HRE1 modulates ethylene responses during hypoxia in Arabidopsis. Plant Physiol. 2011:**156**(1):202–212. https://doi.org/10.1104/pp.111.172486

Yoshida T, Fujita Y, Sayama H, Kidokoro S, Maruyama K, Mizoi J, Shinozaki K, Yamaguchi-Shinozaki K. AREB1, AREB2, and ABF3 are master transcription factors that cooperatively regulate ABRE-dependent ABA signaling involved in drought stress tolerance and require ABA for full activation. Plant J. 2010:**61**(4):672–685. https://doi.org/10.1111/j.1365-313X.2009.04092.x

Zhang B, Horvath S. A general framework for weighted gene co-expression network analysis. Stat Appl Genet Mol Biol. 2005:**4**:Article17. https://doi.org/10.2202/1544-6115.1128

Zhang Y, Liu Y, Sun L, Baskin CC, Baskin JM, Cao M, Yang J. Seed dormancy in space and time: global distribution, paleoclimatic and present climatic drivers, and evolutionary adaptations. New Phytol. 2022:**234**(5):1770–1781. https://doi.org/10.1111/nph.18099